

## Reply to Reviewer #1

We are thankful to Reviewer #1 for his/her comments and suggestions.

The comments from Reviewer #1 are in italics followed by our responses:

*1. To the first part of the paper, regarding the comparison of models and observations:*

*- While the authors document significant difference between their model and observations for the chosen time period, it is hard to interpret the results without some knowledge of natural variation in aerosol loading in the region. A brief discussion on this, e.g. including some climatology of AODs from MODIS or AeroNet, would be beneficial to the reader her.*

Following the reviewer's suggestions, we added a new paragraph describing the regional AOD climatology from MODIS as the new first paragraph of Section 3.1 after the first sentence "The model simulations of monthly mean AOD for March 2012 are compared with the MODIS/Terra satellite observations in Fig. 1" on Line 15, Page 16910, as follows:

"...During this time of the year, the Indo-Ganges Valley is impacted with locally emitted aerosols from urban and industrial sources as well as dust mainly from nearby arid agricultural lands and deserts (Giles et al., 2011). As shown in Fig. 1a, the MODIS retrievals of AOD are generally larger than 0.5 in these areas. Given the dry pre-monsoon conditions with small wet removal, these aerosols are transported in long distance by the northwesterly winds prevailing in the Valley. That leads to similarly high AODs (>0.5) over to the Bay of Bengal and the eastern India in the MODIS observations. Another aerosol hotspot is off the southwest coast of the Indian subcontinent, influenced by both nearby anthropogenic emissions in the western India and long-range transported pollutions from the northern India (Ramanathan et al., 2001). Dust dominates the AOD observed over the Arabian Sea with values about 0.3~0.5."

Some portion of the discussions on differences between the model results and MODIS AOD in the same paragraph of Section 3.1 (from Line 15, Page 16910 to Line 3, Page 16911) are revised accordingly to exclude the repetitions from the new additions above, as follows:

"The model-calculated AODs (shown in Fig. 1b) are lower than MODIS retrievals over most of the domain, while the overall geographic pattern of AOD distributions is simulated except for over the Arabian Sea. Large AODs are predicted in northern and eastern India and along the pathway that the aerosol plumes travel to southwestern India and the downwind as depicted similarly in the MODIS observations. But the maximum AOD values calculated by the model are much lower around 0.3~0.4. AODs less than 0.1 are predicted over most of northwestern India and the adjacent oceans, whereas MODIS has much higher values (> 0.3). ..."

Additionally, we added a new sentence to the second paragraph of Section 3.1, on Line 14, Page 16911, to describe AOD climatology at two ground sites: Nainital and Kanpur, as follows:

"...nearby Kanpur (~390 km southeast; the two sites are marked in Fig. 1b). Being a relatively clean site, Nainital has a monthly mean AOD of 0.232 from MFRSR measurements, while the mean AERONET AOD is 0.583 at Kanpur. The discrepancies between the modeled and observed AOD are much smaller at the Nainital site in Fig. 1d..."

*2. The authors provide some indication of the uncertainty on the CALIPSO data, but apart from this there is little evaluation of the significance of the differences found between models and data - e.g. in*

Table 1 and Figure 2. An assertion that a significance test has indeed been performed should be added here.

The following statement on significance tests is now added to the end of the second paragraph of section 3.2, on Line 11, Page 16913, following the discussions on Table 1 and Figure 2:

“...available on the regional scale. Two-sample t-test of extinction time series suggests that the differences between the model calculations and observations (MPL data for Nainital and Kanpur; and CALIPSO data for South Asia) are significant below 2.5 km with p-values less than the significance level of 0.05.”

Additionally, significance test results are provided below for Reviewer’s reference. Figure R.1 below shows the calculated monthly mean and standard deviation of modeled and observed daily aerosol extinction profiles for Nainital, Kanpur, and South Asia, respectively. Since there are only 3 and 4 CALIPSO tracks with valid retrievals over Nainital and Kanpur in March 2012 (as given in Table 2; numbers in parentheses), the ground-based MPL profiles are shown for those two ground sites instead of CALIPSO retrievals and used in the t-test. This figure shows that the model means  $\pm$  standard deviations are less than the observed means below 2.5km for all three locations.

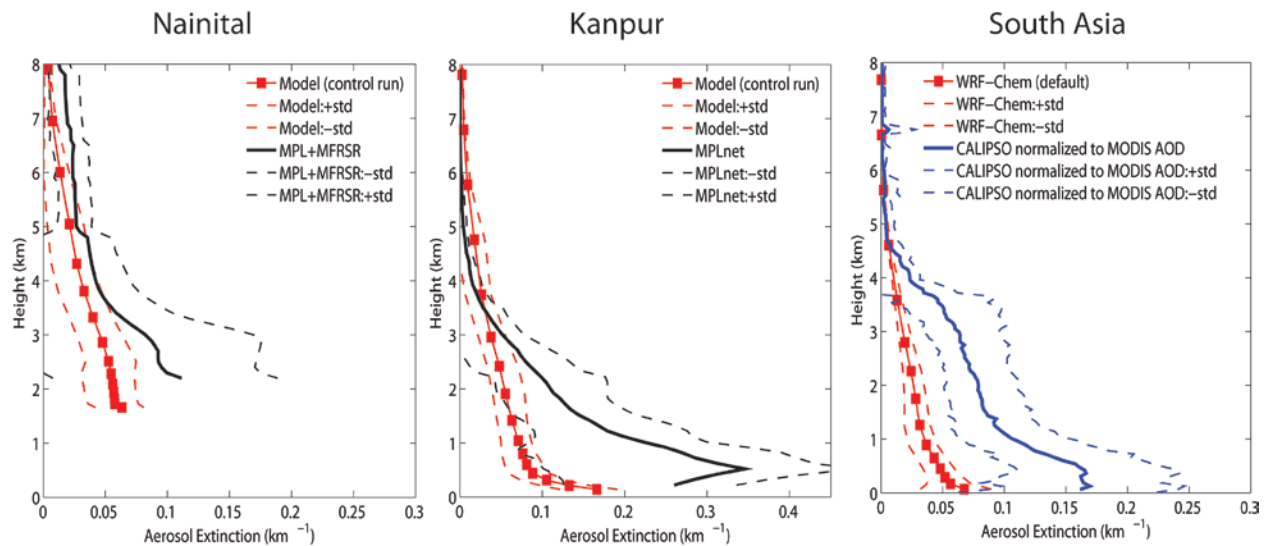


Figure R.1 Monthly mean and mean  $\pm$ standard deviation of modeled and observed daily aerosol extinction profiles for Nainital, Kanpur, and South Asia, respectively

Furthermore, the p-values calculated in the t-test for a selection of altitudes are listed in the table below for each location. It suggests that below 2.5km, the model and observed extinctions are statistically different with a p-value less than 0.05.

Nainital Z(km)	2.3	2.5	2.9	3.3	3.8	4.3	5
P value	0.009	0.0489	0.112	0.128	0.188	0.115	0.207

Kanpur Z(km)	0.2	0.6	1.4	2.4	3.	3.7	4.8
P value	8e-8	1e09	1.9e-7	0.004	0.10	0.31	0.005

South Asia Z(km)	0.2	0.7	1.3	2.3	2.8	3.6	4.6
P value	0.	0.	0.	0.	0.	0.	0.06

3. To the second part, on the radiative and thermodynamic responses to the different aerosol profiles:

- For the results shown in Figures 5, 6 and 7, it is hard to assess whether the differences found are actually due to the changes to the aerosol profiles, or to internal variability in the modelled climate system. While the focus here is on the difference between the extinction profiles, under identical climate conditions, running e.g. three perturbed ensemble members for each profile for the selected month would greatly strengthen the impact of these figures. I would urge the authors to consider this, even if it means spending some extra computational time.

We would like to clarify that for the results shown in Figures 5, 6 and 7, differences found between the three cases (control run, case I, and case II) are due to the changes to the aerosol profiles, because they all deviate from the same base simulation without aerosols and the only difference between the three cases is the aerosol profile used. These differences, as also noted by the reviewer, are the focus of this study, and they are not directly related to the model internal variability.

The model internal variability may affect the results of each case (control run, case I, and case II), which represent the absolute aerosol effects simulated. While we agree with the reviewer that the ensemble mean is helpful to quantify the absolute aerosol effects (also a longer simulation period may be necessary), we do not think that it would help much on our focus on the differences between the absolute aerosol effects.

To account for this point raised by the reviewer, we revised the sentence in the Section 4, Summary and discussion, (Lines 28-29, Page 16923) from:

“...It would be desirable to conduct similar evaluations for longer times to better investigate the climate response to uncertainties in modeled aerosols...”

to:

“...It would be desirable to conduct similar evaluations for longer times and use ensemble members of perturbed meteorological conditions to better investigate the climate response to uncertainties in modeled aerosols...”

4. Page 16915, line 27: “Therefore, the largest warming is calculated for Case I”. Given the almost vanishing temperature response over oceans here, and the closeness of the three curves in Figure 3, is this statement statistically valid?

Agreed that the differences in temperature responses over oceans are small between three cases in Figure 3, because of the fixed sea surface temperature. This sentence on Page 16915, line 27 is now removed.

## Reply to Reviewer #2

We are thankful to Reviewer #2 for his/her comments and suggestions.

The comments from Reviewer #2 are in italics followed by our responses:

*Specific comments:*

- 1. In section 3.1, authors evaluated model simulated AOD using MODIS derived AOD and found that model underestimate the AOD by a factor of 2. Model is not able to capture the high AOD belt over Indo-Gangetic Plain (IGP) and most of northern parts of India (Figure 1). Dust transport from West Asia (MODIS AOD) is also not captured in the modelled AOD (Figure 1). Authors need to check dust emission flux to figure out how well model able to simulate dust source regions. A brief discussion about species-wise AOD information could be useful for explaining the underestimation of model simulated AOD.*

We agree with the reviewer that emissions may contribute to the underestimation of AOD. For the dust emissions used in this study, it is described in the Section 2.1, Lines 18-19, on Page 16907,

“Dimethyl sulfide, dust, and sea salt emissions are calculated online as for the GOCART model (Ginoux et al., 2001; Chin et al., 2002)”.

And also, this dust emission scheme, which is implemented in the WRF-Chem (MOZCART) that we use, has been evaluated extensively over India by Kumar et al. (2014). Therefore, we cited that paper in the Section 2.1, Lines 3-5, on Page 16907,

“This version of the WRF-Chem aerosol and chemistry modules has been used and evaluated in studying effects of dust aerosols on tropospheric chemistry during the pre-monsoon season in northern India (Kumar et al., 2014)”

Other factors such as meteorological conditions (such as relative humidity, boundary layer dynamics and soil moisture in the case of dust) could also contribute to the AOD underestimation in addition to emissions. However, a comprehensive analysis of model schemes and boundary conditions is required to provide such information. We think that it is beyond the scope of this paper. This limitation and the main goal of the current study are given on Lines 10-13, Page 16922,

“Resolving the mismatch between simulated and observed aerosol extinction profiles requires possible upgrades of multiple model physics schemes and quantification of key parameters that could affect vertical distribution of aerosols, for instance, biomass burning injection heights (Grell et al., 2011), boundary layer height and near-surface winds (Nair et al., 2012). Additionally, high-quality measurements at different locations are also needed for model evaluation over longer time periods, and it is recommended for future studies over this region”

To address the contribution to the AOD by individual aerosol species raised by the reviewer, we plot the species-specific aerosol burdens as a proxy for understanding the contribution to the AOD by individual aerosol species, since in our model AOD is calculated assuming the internal aerosol mixtures, and the species-specific AOD is not available. Fig. S1 below shows the calculated aerosol burdens for March 2012. This new figure is now included in the Supplementary Material as well as the following discussions:

“In our model, aerosol optical depth (AOD) is calculated with the internal mixing assumption. In order to attribute the AOD underestimation to major aerosol types, we plot the species-specific aerosol burdens as a proxy for understanding the contribution to the AOD by

individual aerosol species. Fig. S1 shows the aerosol burdens calculated for March 2012. Since dust is the dominating species over northwestern India semi-arid regions and the adjacent Arabian Sea, it is the main contributor to the underestimation of AOD over these regions. In contrast, anthropogenic sulfate, oc, and bc are the main components of aerosol loadings (thus AOD) in polluted northern and northeastern India, as well as in the long-distance transported aerosols over the downwind of southwestern Indian sub-continent.”

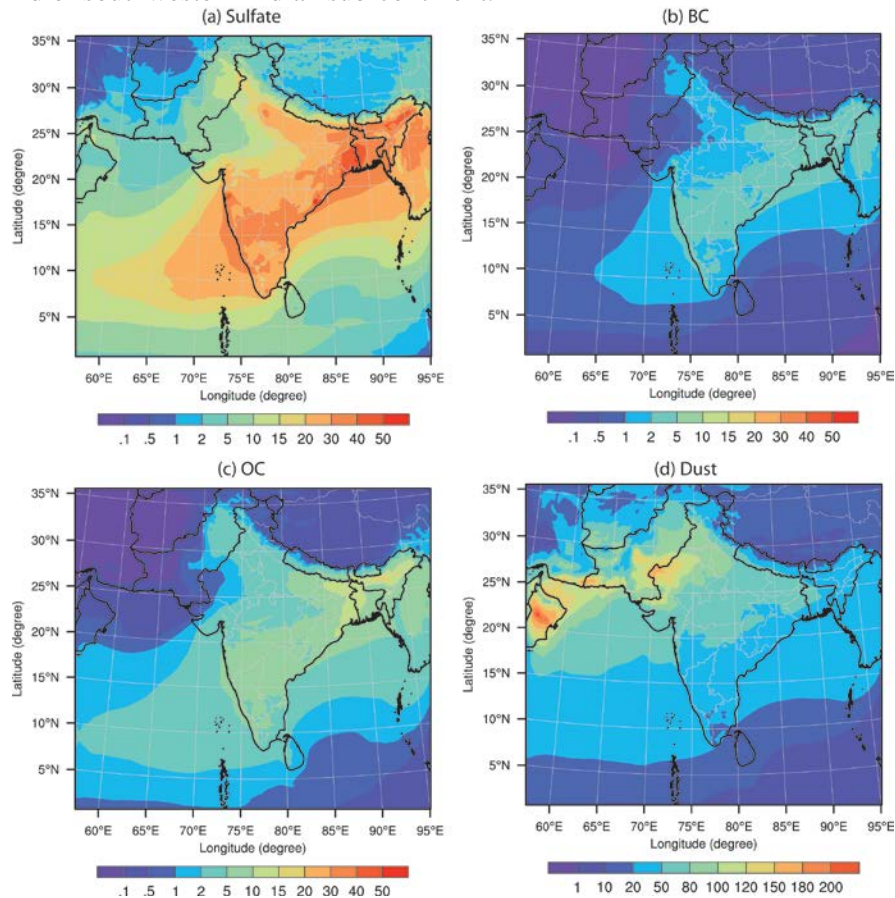


Figure S1. Calculated aerosol burdens (mg/m<sup>2</sup>) of (a) Sulfate, (b) BC, (c) OC, and (d) Dust for March 2012

We also added the following additional discussions in the text, Section 3.1, Lines 1-3 on Page 16911 as follows,

“These discrepancies could be attributable to episodic dust activities not reproduced by WRF-Chem (as shown in Fig. S1 that dust aerosols are dominating species) or to overestimation associated with the MODIS satellite retrievals over highly reflective surfaces such as deserts and clouds over the ocean. In other aerosol-concentrated areas, anthropogenic pollutants such as sulfate, BC, and OC are the main contributors to the AOD underestimation (Fig. S1)”

2. *Authors discussed the evaluation of modelled AOD for March 2012, even though the simulations are available for eight months (From August 2011 to March 2012). It would useful if authors use the entire simulation period for the model evaluation.*

The reason that we only presented the AOD comparison for March 2012 is because the ground-based lidar observations of aerosol vertical profiles are available only for that month. Since the objective of this paper is to “identify altitude-related bias” and examine the subsequent responses due to the mis-represented vertical profiles of aerosol extinctions, we decided not to include the model results of AOD from other months for which we do not have vertical profile measurements to evaluate. Justifications of limiting our analysis to one month (March 2012) were given in Section 2.1, Lines 12-17, on Page 16908,

“The model-data analysis and discussions here center on simulations in March 2012, for two reasons. First, during this pre-monsoon month, ground-based lidar measurements are available at Nainital and Kanpur (in northern India) and used with satellite observations to characterize bias in the calculated aerosol extinctions. As discussed later, it is important to have independently calibrated ground-based measurements because of the uncertainty associated with satellite data.”

For the reviewer’s reference, the AOD comparison for other months is shown below in Fig. R2.1. It indicates underestimation in the model-calculated AOD similar to that for March 2012. Resolving these mismatches between simulated and observed AOD requires development of a verification database extending from field campaigns, ground-based and aircraft measurements for evaluation of model simulated boundary layer dynamics and aerosol concentrations and chemical composition. This could then lead to possible upgrades of model physics schemes and quantification of key parameters including emissions, biomass burning injection heights, boundary layer height and near-surface winds etc. We consider that it is beyond the scope of this paper and certainly deserves further investigation.

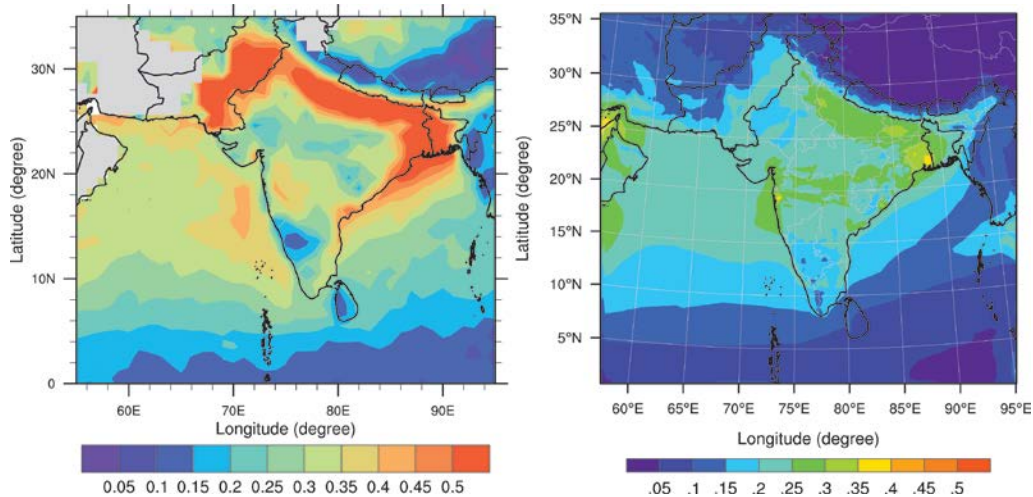


Figure R2.1 Time averaged AOD between Aug 2011 and March 2012 from (left) MODIS/Terra, and (right) WRF-Chem simulations

3. *Authors found that “83% of the model low-bias is due to aerosol extinctions below 2 km”. A brief discussion about the vertical distribution of anthropogenic and wildfire emissions treatment in*

*the model would be useful to the reader here. How this treatment could influence the uncertainty in the vertical distribution of extinction?*

Following the suggestion by the reviewer, we now include the following sentence in the “Methodology” (Section 2.1) describing the vertical distribution of aerosol emission treatment, Line 20, on Page 16907:

“Primary aerosol emissions including all the anthropogenic, biomass burning and natural sources are injected into the lowest level of the model and transported by advection and updrafts. Calculations of optical properties of aerosol assume...”

We also add more and revise the following discussions in the “Summary and Discussion” (Section 4), Lines 10-13, on Page 16922:

“Resolving the mismatch between simulated and observed aerosol extinction profiles requires possible upgrades of multiple model physics schemes and quantification of key parameters that could affect vertical distribution of aerosols, for instance, biomass burning injection heights (Grell et al., 2011), boundary layer height and near-surface winds (Nair et al., 2012) as well as a. Additionally, high-quality measurements at different locations are also needed for model evaluation over longer time periods, and it is recommended for future studies over this region”

It should also be noted that the biomass-burning source over this region is primarily due to seasonal burning of agriculture waste concentrated over the agricultural region to the west and during December and early January (first crop also known as kharif). A second crop is also harvested during spring and is associated with biomass burning peaks in April/May (Rabi crops).

Two references added:

Grell, G., Freitas, S. R., Stuefer, M., and Fast, J.: Inclusion of biomass burning in WRF-Chem: impact of wildfires on weather forecasts, *Atmos. Chem. Phys.*, 11, 5289-5303, 2011.

Nair, V. S., Solmon, F., Giorgi, F., Mariotti, L., Babu, S. S., and Moorthy, K. K.: Simulation of South Asian aerosols for regional climate studies, *J. Geophys. Res.*, 117, D04209, doi:10.1029/2011JD016711, 2012.

4. *Authors separated the effect of absorption and scattering properties using two simulations (Case 1 and Case 2). But between Case 1 and Case 2, there can be considerable changes to the aerosol distributions. How does this contribute to the uncertainty in simulated aerosol extinction profiles?*

As described in the Section 3.2, Lines 12-17, on Page 16913, sensitivity studies including both Case I and Case II are conducted by “optimizing matching of the observed aerosol vertical profiles. The calculated aerosol extinctions in the lowest eight model layers (below ~850 hPa, at 1.5-3 km above sea level in the simulated model domain) are increased by a factor of 2 at each time step...” That means that in both sensitivity cases, the simulated aerosol concentrations are kept the same as in the control run, and aerosol extinction profiles (sum of scattering and

absorption) were adjusted to the same level (i.e., a factor of 2 increases), although their scattering or absorbing fractions are different.

This is clearly shown in the model results as in Fig. 1(c) for AOD and Fig. 2 for extinction profiles. Only one curve is needed on each panel to represent the results from sensitivity studies (both Case I and Case II) labeled as “Double extinction below 850 hPa” in Fig. 1(c) and “Model (increased ext)” in Fig. 2”. We have also clarified this point in the discussions of results, Section 3.3, Lines 15-17, on Page 16915,

“Because aerosol extinctions (thus AODs) in Cases I and II are increased to the same level, the TOA radiative effects of aerosols are similar for the two cases...”

And in the Section 3.4, Line 7, on Page 16917,

“Forced by the same aerosol extinction profiles with the bias correction...”

Therefore, the calculated AOD distributions and extinction profiles are identical for Case I and Case II. There are no “considerable changes to the aerosol distributions” nor “contribute to the uncertainty in simulated aerosol extinction profiles” between Case I and Case II.

*Technical comments:*

*Page 16903, Line 26: Wrong citation year (Pan et al., 2015).*

Corrected.

*Page 16905, Lines 10-14: Recent multi-model evaluation paper (Quennehen et al., 2015) is missing from the manuscript.*

Reference Quennehen et al. (2015) is now added as follows on Line 14, Page 16905:

“A recent study by Quennehen et al. (2015) examined six global and one regional models with CALIPSO-derived backscatter profiles at 532nm during August and September 2008, and the multi-model mean backscatter is also underestimated between 0 and 2 km over northern India and eastern China.”

*Page 16907, Lines 15: Compiled SO2 emissions is confusing. Rewrite the sentence.*

It is now revised as follows:

“The total SO<sub>2</sub> emissions in South Asia with updated emissions over India are 9.36 Gg yr<sup>-1</sup>, slightly less than the default GOCART emissions (10 Gg yr<sup>-1</sup>)”

*Page 16910, Lines 17: The geographic pattern of AOD distributions is not reasonably well captured. Rewrite the sentence.*

It is now revised as:

“...the overall geographic pattern of AOD distributions is simulated reasonably well except for over the Arabian Sea”

*Figure 2: Why MPL data extinction profiles peak is different than other data sets?*



The MPL profile at Nainital in Figure 2(a) is similar to other data sets. So we assume that the reviewer refers to the monthly mean MPL extinction profile depicted in the Figure 2(b) for Kanpur, which has a peak around 600m above the surface different from the CALIPSO data and model results. This MPL extinction profile is derived by monthly averaging the quality-assured MPLNET level 2 daytime products (Welton et al., 2001). As shown below (Fig. R2.2) for the 23 days in March 2012 with data available, these MPL daily profiles downloaded from their data archive also have a peak around 600m above the surface, and the reason is not clear from the MPLNET website. Nevertheless, this does not affect our method and main conclusions, since we did not try to match the MPL profiles but applied a systematical bias correction of a factor of 2 to the model predictions below 850hPa.

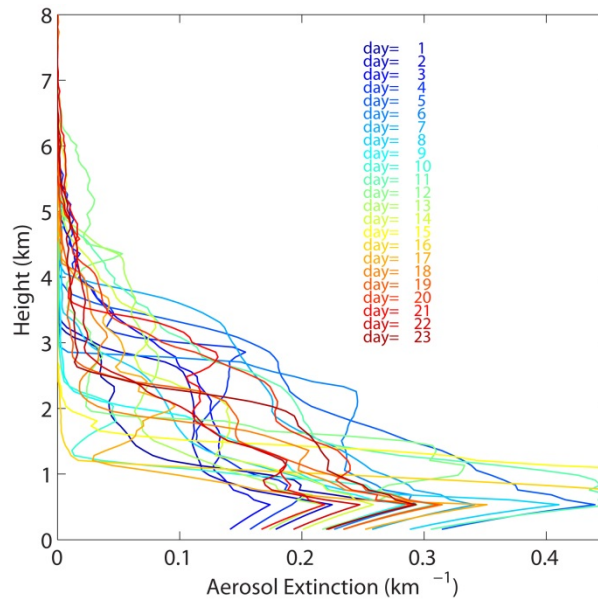


Figure R2.2 MPL daily profiles available from the MPLNET for 23 days in March 2012 at Kanpur

1 **Radiative and Thermodynamic Responses to Aerosol Extinction Profiles during the**  
2 **Pre-monsoon Month over South Asia**

3

4 Y. Feng<sup>1\*</sup>, V. R. Kotamarthi<sup>1</sup>, R. Coulter<sup>1</sup>, C. Zhao<sup>2</sup>, and M. Cadetdu<sup>1</sup>

5

6 <sup>1</sup>Environmental Science Division, Argonne National Laboratory, Argonne, IL

7 <sup>2</sup>Atmospheric Science and Global Change Division, Pacific Northwest National Laboratory,

8 Richland, WA

9 \*e-mail: [yfeng@anl.gov](mailto:yfeng@anl.gov)

10 **Abstract.** Aerosol radiative effects and thermodynamic responses over South Asia are  
11 examined with the Weather Research and Forecasting model coupled with Chemistry  
12 (WRF-Chem) for March 2012. Model results of Aerosol Optical Depths (AOD) and  
13 extinction profiles are analyzed and compared to satellite retrievals and two ground-based  
14 lidars located in the northern India. The WRF-Chem model is found to heavily underestimate  
15 the AOD during the simulated pre-monsoon month and about 83% of the model low-bias is  
16 due to aerosol extinctions below ~2 km. Doubling the calculated aerosol extinctions below  
17 850 hPa generates much better agreement with the observed AOD and extinction profiles  
18 averaged over South Asia. To separate the effect of absorption and scattering properties, two  
19 runs were conducted: in one run (Case I), the calculated scattering and absorption coefficients  
20 were increased proportionally, while in the second run (Case II) only the calculated aerosol  
21 scattering coefficient was increased. With the same AOD and extinction profiles, the two runs  
22 produce significantly different radiative effects over land and oceans. On the regional mean  
23 basis, Case I generates 48% more heating in the atmosphere and 21% more dimming at the  
24 surface than Case II. Case I also produces stronger cooling responses over the land from the  
25 longwave radiation adjustment and boundary layer mixing. These rapid adjustments offset the  
26 stronger radiative heating in Case I and lead to an overall lower-troposphere cooling up to  
27  $-0.7 \text{ K day}^{-1}$ , which is smaller than that in Case II. Over the ocean, direct radiative effects  
28 dominate the heating rate changes in the lower atmosphere lacking such surface and lower  
29 atmosphere adjustments due to fixed sea surface temperature, and the strongest atmospheric  
30 warming is obtained in Case I. Consequently, atmospheric dynamics (boundary layer heights  
31 and meridional circulation) and thermodynamic processes (water vapor and cloudiness) are  
32 shown to respond differently between Case I and Case II underlying the importance of  
33 determining the exact portion of scattering or absorbing aerosols that lead to the  
34 underestimation of aerosol optical depth in the model. In addition, the model results suggest  
35 that both direct radiative effect and rapid thermodynamic responses need to be quantified for  
36 understanding aerosol radiative impacts.  
37

## 1. Introduction

South Asia, including the Indian subcontinent and adjacent oceans, is a regional hotspot with high aerosol loadings (Ramanathan et al., 2001; Moorthy et al., 2013). Aerosols over this region are composed of locally emitted sulfate, black carbon (BC), and organic substances (mainly from industrial, transportation, residential, and agricultural burning), as well as long-range-transported desert dust and sea spray aerosols. These aerosols together induce a large negative radiative forcing at the top of the atmosphere (TOA) through direct scattering and absorption of incoming solar radiation. With year 2000 emissions, Chung et al. (2010) estimated the regional TOA aerosol forcing in South Asia at about  $-1.9 \text{ W m}^{-2}$ , which is larger by several factors than the present-day global mean direct forcing (Boucher et al., 2013). The overall aerosol cooling effect in response to negative TOA forcing is suggested to weaken the sea surface temperature gradient over the Indian Ocean and decelerate the monsoonal circulation and moisture transport (Ramanathan et al., 2005). Other studies show that local warming by BC in the upper troposphere intensifies vertical motion over land and modulates intraseasonal monsoon rainfall variations (Lau et al., 2006). Therefore, rapidly increased anthropogenic aerosol emissions in South Asia have been linked closely to observed changes in surface temperature and rainfall patterns in global climate simulations (Meehl et al., 2008; Lau et al., 2009; Wang et al., 2009; Bollasina et al., 2011; Ganguly et al., 2012).

For quantifying aerosol direct perturbations in the radiation budget, column-integrated aerosol optical depth (AOD) is often examined in global models, some of which include regional analysis over South Asia (Myhre et al., 2009, 2013; Shindell et al., 2013; Boucher et al., 2013; Pan et al., 2015), and in regional-scale models (Chung et al., 2010; Nair et al., 2012; Kumar et al., 2014). Besides AOD, aerosol single scattering albedo (SSA) has also been identified as a main source of uncertainty in estimates of aerosol direct forcing (McComiskey et al., 2008; Loeb and Su et al., 2010) and evaluated with observations. Most models underpredict aerosol abundances over South Asia versus data from the ground-based Aerosol Robotic Network (AERONET) (Holben et al., 1998) or satellite-retrieved AOD observations such as the Moderate Resolution Imaging Spectroradiometer (MODIS) (e.g., Yu et al., 2003; Kinne et al., 2006; Koch et al., 2009; Ganguly et al., 2012). In addition, models

68 also tend to underestimate aerosol absorption by over-estimating the SSA (Liu et al., 2012).  
69 Such low biases in aerosol optical properties might potentially affect model simulations of  
70 regional climatology and assessment of aerosol climate impacts over the South Asia region.

71 Vertical distribution of aerosols is another important parameter in determining  
72 aerosol-radiation interactions. When column AOD is constrained, uncertainties in aerosol  
73 vertical profiles can still contribute to significant uncertainties in the calculation of radiative  
74 forcing (Lohmann et al., 2001; Zarzycki and Bond, 2010; Ban-Weiss et al., 2011). The extent  
75 to which the aerosol profile impacts aerosol radiative effects depends on the presence of  
76 cloud, surface albedo, and SSA. Column and global aerosol and radiation models have been  
77 used to explore the sensitivity of aerosol direct radiative forcing to the vertical distribution of  
78 aerosols, especially absorbing aerosols, relative to clouds (Haywood and Shine, 1997; Liao  
79 and Seinfeld, 1998; Samset et al., 2013; Vuolo et al., 2014; Choi and Chung, 2014). However,  
80 compared to column AOD and SSA, aerosol vertical distributions are evaluated less  
81 frequently against observations, partly due to lack of observational data sets.

82 Aircraft profiling of aerosol concentrations from recent airborne experiments, such as the  
83 HIAPER Pole-to-Pole Observations (Schwarz et al., 2010) and the Arctic Research of the  
84 Composition of the Troposphere from Aircraft and Satellites (Jacob et al., 2010), provides  
85 high-quality data sets for model comparison (e.g., Koch et al, 2009; Liu et al., 2012).  
86 However, these data sets are usually available only for limited locations and time periods. In  
87 particular, few long-term aircraft surveys are available for South Asia, other than a few past  
88 field experiments such as the Maldives Autonomous Unmanned Aerial Vehicle Campaign  
89 (Ramanathan et al., 2007) and the Integrated Campaign for Aerosol, Gases and Radiation  
90 Budget experiment (Satheesh et al., 2009). Satellite-retrieved aerosol extinction profiles  
91 providing wide coverage in space and time have been used increasingly for model evaluation.  
92 Using the Cloud-Aerosol Lidar and Infrared Pathfinder Satellite Observations (CALIPSO)  
93 lidar nighttime data at 532 nm in cloud-free conditions from June 2006 to November 2007,  
94 Yu et al. (2010) evaluated aerosol extinction profiles simulated by the Goddard Chemistry  
95 Aerosol Radiation Transport (GOCART) model and found substantial underestimation in the  
96 magnitude of aerosol extinctions over the Indian subcontinent. Similar analysis of all-sky  
97 CALIPSO nighttime data in the AeroCom (Aerosol Comparisons between Observations and

98 Models) multi-model evaluation of the vertical distribution of aerosols (Koffi et al., 2012)  
99 found that 11 of the 12 AeroCom models underestimated the annual mean aerosol extinctions  
100 below 2 km over South Asia. [A recent study by Quennehen et al. \(2015\) examined six global  
101 and one regional models with CALIPSO-derived backscatter profiles at 532nm during August  
102 and September 2008, and the multi-model mean backscatter is also underestimated between 0  
103 and 2 km over northern India and eastern China.](#)

104 Although these model-data comparisons help to identify the biases in model simulations  
105 of aerosol extinction or concentration profiles, the resultant changes in atmospheric heating,  
106 dynamics, and cloud adjustments (the aerosol semi-direct effects) have yet to be investigated.  
107 Moreover, satellite retrievals of aerosol extinction profiles are also subject to uncertainties  
108 associated with cloud contamination, surface overlap correction, and daylight background  
109 noise. Observational studies have examined atmospheric heating rates extensively by using  
110 aerosol extinctions retrieved from ground-based or CALIPSO lidar instruments (Misra et al.,  
111 2012; Gautam et al., 2010; Kuhlmann and Quaas, 2010) and *in situ* aircraft data (Ramana et  
112 al., 2007; Satheesh et al., 2008). These studies directly provide observational constraints on  
113 the instantaneous atmospheric heating caused by aerosols, ranging from 0.35 to 2 K day<sup>-1</sup>, in  
114 the South Asia region. On the other hand, observational methods face challenges in  
115 distinguishing the rapid adjustments in the atmosphere attributable to aerosols versus other  
116 environmental influences.

117 In the present study, we examine the atmospheric radiative and thermodynamic responses  
118 to uncertainty associated with vertical distributions of aerosol extinction coefficient by  
119 correcting bias in model calculations with satellite and surface remote sensing data. This not  
120 only identifies discrepancies between the model-predicted and observed aerosol optical  
121 properties as a function of height, but it also demonstrates the potential importance of  
122 aerosol-related uncertainty for regional climate simulations. The regional Weather Research  
123 and Forecasting (WRF) model, coupled with a chemistry module (WRF-Chem), is used to  
124 simulate the pre-monsoon month of March 2012 over South Asia. The next section describes  
125 the regional climate model configurations and ground-based and satellite data sets available.  
126 Section 3 evaluates the modeled and observed AODs and aerosol profiles and discusses  
127 changes in the simulated radiative energy balance, surface temperature, lower-atmospheric

128 heating rates, boundary layer (BL) height, large-scale circulation, and cloud occurrence, in  
129 response to optimized matching of aerosol extinction profiles to observations. The main  
130 findings of this study and implications for future work are summarized in Section 4.

## 131 **2. Methodology**

### 132 **2.1 Model description**

133 This study uses a version of the WRF-Chem 3.3 (Skamarock et al., 2008; Grell et al.,  
134 2005), coupled with the chemistry module MOZCART (Pfister et al., 2011), to simulate  
135 aerosol distributions, aerosol-radiation interactions, and regional meteorological fields. The  
136 default model simulations are performed for eight months from August 2011 to March 2012,  
137 the period when multi-instrumental aerosol observations were collected by the U.S.  
138 Department of Energy (DOE) Ganges Valley Aerosol Experiment (GVAX) at a mountain-top  
139 site, Nainital (29°N, 79°E, e.s.l. 1939 m), in northern India. The model domain is configured  
140 from 55°E to 95°E and 0° to 36°N, with a horizontal grid spacing of ~12 km and 27 vertical  
141 layers. The MOZCART chemistry module (Kumar et al., 2014) includes the MOZART-4  
142 gas-phase chemistry (Emmons et al., 2010) and the GOCART bulk aerosol scheme (Chin et  
143 al., 2002). MOZCART simulates externally mixed aerosol species including sulfate, BC,  
144 organic carbon (OC), dust (in 5 size bins with 0.5, 1.4, 2.4, 4.5, and 8  $\mu\text{m}$  effective radius)  
145 and sea salt (in 4 size bins with 0.3, 1.0, 3.2, and 7.5  $\mu\text{m}$  effective radius). This version of the  
146 WRF-Chem aerosol and chemistry modules has been used and evaluated in studying effects  
147 of dust aerosols on tropospheric chemistry during the pre-monsoon season in northern India  
148 (Kumar et al., 2014).

149 The anthropogenic emissions of gaseous species are derived from the Reanalysis of the  
150 Tropospheric Chemical Composition and Emissions Database for Global Atmospheric  
151 Research compiled for the year 2000. The default emissions of BC, OC, and  $\text{SO}_2$  are same as  
152 in the GOCART model for year 2006. Over India, emissions of BC, OC, and  $\text{SO}_2$  are  
153 replaced with year 2010 inventories available at resolutions of  $0.1^\circ \times 0.1^\circ$  for anthropogenic  
154 sources and  $0.5^\circ \times 0.5^\circ$  for biomass burning (Lu et al., 2011). The total emissions of BC and  
155 OC used in this study are about 1.12 Gg/yr and 3.06 Gg/yr over India, respectively, roughly  
156 51% and 63% higher than those from the default GOCART global inventories (0.74 Gg/yr  
157 and 1.88 Gg/yr). The [total SO2 emissions in South Asia with updated emissions over India](#)

158 [are 9.36 Gg yr<sup>-1</sup>, slightly less than the default GOCART emissions \(10 Gg yr<sup>-1</sup>\).](#) ~~compiled~~  
159 ~~SO<sub>2</sub> emissions of 9.36 Gg/yr are comparable to the GOCART emissions (10 Gg/yr).~~  
160 Additional sulfate emissions from waste and biofuel burning (Yevich and Logan, 2003) are  
161 also included (about 0.21 Gg/yr). Dimethyl sulfide, dust, and sea salt emissions are calculated  
162 online as for the GOCART model (Ginoux et al., 2001; Chin et al., 2002). [Primary aerosol](#)  
163 [emissions including all the anthropogenic, biomass burning and natural sources are injected](#)  
164 [into the lowest level of the model and transported by advection and updrafts.](#) Calculations of  
165 optical properties of aerosols assume internal mixing (Fast et al., 2006), including the  
166 Kappa-based hygroscopic growth of aerosol components (Petters and Kreidenweis, 2007).  
167 The Rapid Radiative Transfer Model for General Circulation Model schemes (Iacono et al.,  
168 2008) is used for shortwave and longwave radiation calculations (Zhao et al., 2011). Other  
169 main physical packages used in this study are the Thompson cloud microphysics (Thompson  
170 et al., 2008), the Zhang-McFarlane cumulus parameterization (Zhang and McFarlane, 1995),  
171 the Mellor-Yamada-Janjic BL scheme (Janjic, 1994), and the Rapid Update Cycle land  
172 surface model (Benjamin et al., 2004).

173 The initial and boundary conditions of meteorological fields were interpolated to the  
174 model time step (72 s) from the compiled 6-h National Centers for Environmental Prediction  
175 reanalysis data available at 1° × 1° resolution. Outputs from the MOZART-4 global chemical  
176 transport model (Emmons et al., 2010) generated for the simulation time periods are used for  
177 chemistry initial and boundary conditions. Radiative feedbacks of aerosols are coupled with  
178 the meteorology updates at each model time step. Indirect aerosol microphysical effects are  
179 not considered. While this omission might affect the simulated total aerosol radiative impact,  
180 the focus here is on examination of the model's sensitivity to uncertainty in predicted aerosol  
181 extinction, which, as an aerosol optical property, has a direct impact on aerosol direct and  
182 semi-direct radiative effects more than aerosol microphysical effect.

183 The model-data analysis and discussions here center on simulations in March 2012, for  
184 two reasons. First, during this pre-monsoon month, ground-based lidar measurements are  
185 available at Nainital and Kanpur (in northern India) and used with satellite observations to  
186 characterize bias in the calculated aerosol extinctions. As discussed later, it is important to  
187 have independently calibrated ground-based measurements because of the uncertainty



188 associated with satellite data. Second, we examine the model's performance in simulating  
189 AOD and vertical distributions for this pre-monsoon month, because the anthropogenic  
190 aerosol concentrations over this period are among the highest of the year and impose large  
191 radiative forcing (Ramanathan et al., 2007). Uncertainty in aerosol predictions might  
192 propagate into the predicted meteorological fields and influence the moisture distribution in  
193 the pre-monsoon-to-monsoon season. In addition to the default (control) run for March, two  
194 sensitivity model simulations are conducted with corrected extinction profiles, as described  
195 below. One-week spin-up is used for initializing the one-month runs.

## 196 **2.2 Observational data sets**

197 During the GVAX experiment, the DOE Atmospheric Radiation Measurements (ARM)  
198 Program Mobile Facility 1 (AMF-1) was operated at Nainital in the central Himalayan region  
199 of the northern India. Located at ~1939 m above sea level, this site was frequently near the  
200 planetary BL top or in the free troposphere during the experimental period. Ground-based  
201 AMF-1 multi-filter rotating shadowband radiometer (MFRSR) measurements were made  
202 from September 2011 to March 2012. The post-processed, quality-assured AOD products  
203 (pghmfrsraod1michM1.s1) from the MFRSR are used to evaluate the model simulations of  
204 monthly and daily mean daytime (0600-1800 local time) AODs. Instrumental uncertainty in  
205 the MFRSR-retrieved AOD is about 0.026 above 380 nm (Schmid et al., 1999), which is  
206 generally below the typical AOD levels observed at this site. Monthly mean AERONET  
207 (Holben et al., 1998) level 2 sun photometer AOD data sets that are also used have a reported  
208 uncertainty of approximately 0.01 at 500 nm (Eck et al., 1999; Smirnov et al., 2000).  
209 Comparisons of the simulated monthly mean AODs with Moderate Resolution Imaging  
210 Spectroradiometer (MODIS)/Terra satellite observations (MOD08 Level 3, edition 5; Platnick  
211 et al., 2003) are used to evaluate the geographic distribution of AOD.

212 Vertical profiles of aerosol extinction at 532 nm are retrieved at Nainital from micropulse  
213 lidar (MPL) backscatter measurements and MFRSR AOD data for March 2012, according to  
214 Kafle and Coulter (2013) and Klett (1981). After exclusion of cloud contamination and  
215 missing data, 26 days of MPL-retrieved extinction profiles remain, 25 of which have valid  
216 data during the daytime when MFRSR AOD retrievals are available. The 30-min-frequency  
217 extinction retrievals are averaged hourly and monthly for model comparison with a vertical

218 resolution of ~500 m. Aerosol extinction profiles at 532 nm are also available at a nearby  
219 low-elevation site, Kanpur (26.5°N, 80.3°E, e.s.l. 120m), from the National Aeronautics and  
220 Space Administration's MPL network (MPLNET; Welton et al., 2001). Unlike Nainital,  
221 which is located near the BL top, the Kanpur site provides aerosol characteristics close to the  
222 surface pollution sources in the Indo-Gangetic Basin. During winter and the pre-monsoon  
223 season, this site is often loaded with high concentrations of anthropogenic aerosols mixed  
224 with dust from episodic events (Dey and Di Girolamo, 2010). The quality-assured MPLNET  
225 level 2 daytime products are available from August 2011 to March 2012 for model  
226 comparison. In addition to the ground-based remote sensing data, CALIPSO satellite  
227 retrievals of extinction profiles from the Cloud–Aerosol Lidar with Orthogonal Polarization  
228 sensor (Winker et al., 2009), version 3, level 2, nighttime products are also used to  
229 characterize regional variations in aerosol vertical distribution. Uncertainties associated with  
230 these lidar retrievals of aerosol extinction profiles, either space-borne or ground-based,  
231 include overlapping corrections near the surface, signal-to-noise ratio in the background  
232 (Welton and Campbell, 2002), and propagated errors in AOD measurements (Kafle and  
233 Coulter, 2013). The observations of extinction profiles are used mainly to identify and correct  
234 systematic bias in the model-simulated monthly mean vertical profiles of aerosols. The  
235 aerosol abundances in the column are constrained with column-integrated AOD  
236 measurements from MFRSR and MODIS.

### 237 **3. Results**

#### 238 **3.1 Aerosol optical depth**

239 The model simulations of monthly mean AOD for March 2012 are compared with the  
240 MODIS/Terra satellite observations in Fig. 1. During this time of the year, the Indo-Ganges  
241 Valley is impacted with locally emitted aerosols from urban and industrial sources as well as  
242 dust mainly from nearby arid agricultural lands and deserts (Giles et al., 2011). As shown in  
243 Fig. 1a, the MODIS retrievals of AOD are generally larger than 0.5 in these areas. Given the  
244 dry pre-monsoon conditions with small wet removal, these aerosols are transported in long  
245 distance by the northwesterly winds prevailing in the Valley. That leads to similarly high  
246 AODs (>0.5) over to the Bay of Bengal and the eastern India in the MODIS observations.  
247 Another aerosol hotspot is off the southwest coast of the Indian subcontinent, influenced by

248 both nearby anthropogenic emissions in the western India and long-range transported  
249 pollutions from the northern India (Ramanathan et al., 2001). Dust dominates the AOD  
250 observed over the Arabian Sea with values about 0.3~0.5.

251 ~~Figures 1a and 1b show that predicted~~ The model-calculated AODs (shown in Fig. 1b)  
252 ~~are generally~~ lower than MODIS retrievals over most of the domain of South Asia, while  
253 ~~the overall~~ geographic pattern of AOD distributions is simulated except for over the Arabian  
254 Sea. Local maximum AODs are predicted in northern and eastern India and along the  
255 pathway that the aerosol plumes travel to southwestern India and the downwind as depicted  
256 similarly in both model predictions and the MODIS satellite observations retrievals indicate  
257 ~~that the main aerosol sources are located in northern and southwestern India, though~~ But the  
258 maximum AOD values calculated by the model are much lower around 0.3~0.4, are  
259 ~~associated with different threshold values (~0.5 in MODIS and ~0.25 in WRF Chem).~~  
260 Long-range transport of aerosols by the prevailing northwesterly winds in the Indo-Ganges  
261 Valley, also represented in both the model calculations and the MODIS data, results in  
262 moderately high AODs over the Bay of Bengal. The northeasterly winds recirculate the  
263 aerosols from eastern India over to central India, and further down over to the adjacent  
264 Arabian Sea. Low AODs less than 0.1 values ( $\leq 0.1$ ) are predicted by WRF Chem over most  
265 of northwestern India and the adjacent oceans, whereas MODIS has much some higher values  
266 ( $> 0.34$ ) over the sea. These discrepancies could be attributable to episodic dust activities not  
267 reproduced by WRF-Chem (as shown in Fig. S1 that dust aerosols are dominating species) or  
268 to overestimation associated with the MODIS satellite retrievals over highly reflective  
269 surfaces such as deserts and clouds over the ocean. In other aerosol-concentrated regions,  
270 anthropogenic pollutants such as sulfate, BC, and OC are the main contributors to the AOD  
271 underestimation (Fig. S1).

272 The degree to which the model-calculated AOD is lower than the MODIS data is shown  
273 in Fig. 1c. The figure compares the latitudinal variations in AOD averaged between 60°E and  
274 95°E. The default model (control run) calculations of AOD are systematically smaller than  
275 the MODIS data (by about a factor of 2), from the Equator northward to 27°N (Latitudes  
276 north of 27°N are not shown for the MODIS data, because more than 2/3 of the data are  
277 missing). Despite the underestimation in absolute AODs, a gradient in AOD calculated as a

278 function of latitude is similar to the MODIS observations, increasing by about  $\sim 0.1$  AOD  
279 every  $10^\circ$  in latitude. In addition, ~~comparison of~~ the calculated daily daytime mean AODs are  
280 compared with ground-based GVAX MFRSR measurements at Nainital and AERONET data  
281 at nearby Kanpur ( $\sim 390$  km southeast; the two sites are marked in Fig. 1b). Being a relatively  
282 clean site, Nainital has a monthly mean AOD of 0.232 from MFRSR measurements, while  
283 the mean AERONET AOD is 0.583 at Kanpur. ~~—shows that t~~The discrepancies between the  
284 modeled and observed AOD are much smaller at the Nainital site ~~in~~ in Fig. 1d. The monthly  
285 mean AOD at Nainital is estimated at 0.181 by WRF-Chem — about 22% lower than the  
286 ~~value of 0.232 estimated by~~ MFRSR AOD — and the model-data difference is only 13% if  
287 the outlier on day 27 of the observations is excluded. In contrast, the model's underestimation  
288 at Kanpur is about 54%, which is more close to the zonal-mean differences shown in Fig. 1c.  
289 These differences in AOD comparison imply that WRF-Chem tends to underpredict aerosol  
290 extinction (whose vertical integral is AOD) at lower elevations (in the BL) more than in the  
291 free troposphere over this region, because the Nainital data are more representative of the  
292 atmosphere near or above the BL top.

### 293 3.2 Aerosol extinction profiles

294 To further evaluate the vertical distribution of calculated aerosol extinctions ( $b_{ext}$ ), the  
295 ground-based MPL retrievals available in March at Nainital and Kanpur, along with  
296 CALIPSO satellite retrievals, are used. Figure 2 compares the simulated monthly mean  
297 vertical profiles of  $b_{ext}$  with the observational data sets. Like column-integrated AOD,  
298 calculated aerosol extinctions are also lower at the high-elevation Nainital site (Fig. 2a), at  
299 the polluted surface Kanpur site (Fig. 2b), and as an average over the South Asia region (Fig.  
300 2c). Moreover, the discrepancies between the modeled and observed profiles are larger in the  
301 lower atmosphere, where aerosols are more concentrated (as indicated by larger extinctions),  
302 than at higher altitudes in the free troposphere. These differences are further illustrated in Fig.  
303 2d-f, which shows the percent differences in calculated extinction profiles relative to the  
304 CALIPSO data in the column. Table 1 summarizes the column-mean relative differences (%)  
305 between the predicted monthly mean  $b_{ext}$  and retrievals from the CALIPSO data, expressed  
306 as

$$307 \quad \frac{\sum_{i=1}^n [b_{ext,model(i)} - b_{ext,CALIPSO(i)}]}{n} \times 100, \text{ where } b_{ext,CALIPSO} > 0.01 . \quad (1)$$

308 For altitudes below 850 hPa (or ~2-3 km, depending on the location), the calculated  
 309 average differences between the model control run and the CALIPSO data are -56%, -52%,  
 310 and -77% for Nainital, Kanpur, and South Asia, respectively. In comparison, smaller  
 311 differences of -33%, -33%, and -75%, respectively, are estimated for the entire column.

312 The monthly mean extinction height ( $z_\alpha$ ), defined as  $\frac{\sum_{i=1}^n b_{ext,i} z_i}{\sum_{i=1}^n b_{ext,i}}$  (Koffi et al., 2012), is  
 313 also calculated in order to compare the modeled aerosol mean vertical structure with  
 314 observations (Table 2). On a regional mean basis over South Asia,  $z_\alpha$  estimated from the  
 315 March CALIPSO data is 1.7 km in this study. This value is consistent with the  
 316 March-April-May mean extinction height of 1.99 km given by Koffi et al. (2012). However,  
 317 model estimates of  $z_\alpha$  in the control run are generally higher than those inferred from  
 318 ground- and satellite-based data sets over different locations/areas in South Asia, as shown in  
 319 Table 2. The only exception is the comparison with MPL data at Nainital, with a slightly  
 320 lower model-calculated  $z_\alpha$ . This might be due to spatial averaging differences between the  
 321 12-km grid mean model results and the point-based MPL data, because the comparison of  $z_\alpha$   
 322 with the value estimated from CALIPSO for Nainital points to model overestimation,  
 323 consistent with the other sites. The analysis of extinction profiles confirms model  
 324 underestimation of column AOD in March and moreover, indicates that the low bias in AOD  
 325 arises mainly from calculated lower aerosol burden in the lower atmosphere, which leads to  
 326 an AOD underestimate of > 50%, irrespective of location. These differences between the  
 327 observed and modeled profiles at low altitudes are generally larger than the uncertainties  
 328 associated with ground-based measurements (~40%). Although the CALIPSO satellite  
 329 retrievals indicate uncertainties of ~91% to 110%, at the two ground sites their monthly mean  
 330 values are comparable with the ground-based measurements. This validation provides support  
 331 to the regional mean comparison with the CALIPSO data here, as no sufficient ground-based  
 332 measurements are available on the regional scale. [Two-sample t-test of extinction time series](#)  
 333 [suggests that the differences between the model calculations and observations \(MPL data for](#)  
 334 [Nainital and Kanpur; and CALIPSO data for South Asia\) are significant below 2.5 km with](#)

[p-values less than the significance level of 0.05.](#)

To examine potential impacts on calculated radiative and thermodynamic processes from the underestimation of aerosols, sensitivity model runs are conducted for March 2012 by optimizing matching of the observed aerosol vertical profiles. The calculated aerosol extinctions in the lowest eight model layers (below ~850 hPa, at 1.5-3 km above sea level in the simulated model domain) are increased by a factor of 2 at each time step to reduce the identified low bias. However, there are no independent observations of aerosol absorption vertical profiles to constrain the model. AERONET SSA or the satellite-based absorption AOD retrievals provide constraints for column-integrated absorption properties, but neither of them resolves in altitude. To address this uncertainty, two approaches are tested for adjusting the extinction profiles. In Case I, the calculated scattering and absorption coefficients are increased proportionally, so that the altitude-dependent SSA — the fraction of scattering in total extinction — remains the same as in the control run. This case assumes that the underestimation of AOD is contributed proportionally by both scattering and absorbing aerosol loadings. In Case II, only the calculated aerosol scattering coefficient is increased to compensate for the AOD underpredictions, whereas the absorption coefficient remains the same as in the control run, so that the aerosol SSA is increased. This assumption for example could represent for a case study of the underrepresented hygroscopic growth of aerosol particles postulated in other studies for this region (Pan et al., 2015<sup>4</sup>). Comparing Cases I and II will help to illuminate the impact due to uncertainty in modeled aerosol absorption profiles, when the model representation of aerosol extinction profiles is comparable to observations.

As Fig. 1c shows, the zonal-mean AOD comparison with the MODIS observations as a function of latitude is much improved in the sensitivity studies with the adjusted extinction profiles (red dot-dashed line). The domain-averaged mean AOD is higher at 0.31 compared to the base case value of 0.12, and only about 11% lower than that obtained from the MODIS retrieval (0.35). Similarly, adjustment of the extinction profiles also leads to significant improvement in the comparison with MPL and CALIPSO vertical profiles (Fig. 2 and Table 1). Below 850 hPa, the average percentage differences from the CALIPSO extinction profiles decrease to -12%, -11%, and -30% at Nainital, Kanpur, and South Asia, respectively. The mean errors averaged through the entire column also decrease to -22%, -14%, and -40%,

365 respectively.

366 Some of the remaining differences between the calculated and observed profiles in the  
367 sensitivity studies can be attributed to uncertainty associated with column AOD retrievals by  
368 CALIPSO. When the CALIPSO extinction profiles are normalized to the MODIS AOD data,  
369 the differences between modeled and observed extinction profiles averaged over the South  
370 Asia domain (Figs. 2c and 2f) are decreased to -16% for the entire column and -0.4% below  
371 850 hPa (Table 1). This confirms that the bias correction method introduced in the sensitivity  
372 studies compares better with the observed extinction profiles on the regional scale. On the  
373 other hand, the CALIPSO profile normalized to the column integral of the MPL-retrieved  
374 extinctions at Kanpur results in even larger AOD, thus enlarging the discrepancy from the  
375 predicted extinction profile to -33%. At Nainital, normalization makes little difference,  
376 because the surface and satellite retrievals of column AOD agree well at this site. Overall, at  
377 both ground sites and on the regional mean, the simulations of aerosol extinctions,  
378 particularly near the surface (below 2-3 km), are significantly improved in the sensitivity  
379 studies, compared to the control run. Furthermore, Table 2 shows that, for various regions in  
380 South Asia, the estimated mean extinction height  $z_{\alpha}$  for the adjusted extinction profiles in  
381 the sensitivity studies is generally lowered by about 10-20%. This also results in better  
382 agreement with the CALIPSO-inferred mean extinction heights. In the sections below,  
383 radiative and thermodynamic responses to these improved aerosol extinction profiles are  
384 discussed.

### 385 **3.3 Radiative and surface temperature responses**

386 The buildup of aerosols in March plays an important role in modulating the distribution  
387 of solar radiation throughout the atmosphere over South Asia. In the control run, the  
388 aerosol-induced change in net downward solar radiation at the TOA is estimated at about -3  
389  $\text{W m}^{-2}$ , averaged over South Asia (Table 3), suggesting an overall cooling effect. On the other  
390 hand, aerosols heat the atmosphere by absorbing incoming solar radiation at  $+6.3 \text{ W m}^{-2}$ . This  
391 reduces the net downward radiation at the surface (surface dimming) by  $-9.3 \text{ W m}^{-2}$ . These  
392 estimated changes in radiation fluxes not only account for the instantaneous perturbation on  
393 radiation by aerosols (aerosol direct radiative forcing), but they also include the effects of  
394 rapid responses to aerosols at the land surface and in clouds (semi-direct radiative effects).

395 Because aerosol extinctions (thus AODs) in Cases I and II are increased to the same level, the  
396 TOA radiative effects of aerosols are similar for the two cases, a net reduction of about  $-5 \text{ W m}^{-2}$   
397  $\text{m}^{-2}$ . However, the distribution of incoming solar (shortwave) radiation in the column is very  
398 different between the two cases: the estimated atmospheric absorption is 50% stronger in  
399 Case I, leading to a larger negative aerosol forcing at the surface ( $-14.2 \text{ W m}^{-2}$ ) than in Case II  
400 ( $-11.7 \text{ W m}^{-2}$ ).

401 The aerosol impact on the surface air temperature (at 2 m) in the model simulations,  
402 linked directly to aerosols' perturbation of the radiation budget, is shown in Fig. 3 as a  
403 function of latitude over the land and oceans, respectively. Because the sea surface  
404 temperature is fixed, the surface air temperature over the ocean responds little to aerosol  
405 surface forcing. The near-surface air temperature responds mainly to aerosol heating and  
406 increases in the lower atmosphere over the ocean. ~~Therefore, the largest warming is~~  
407 ~~calculated for Case I.~~ In contrast, the absolute changes in the surface air temperature are  
408 much more significant over the land area, and they are also opposite in sign. Over land, the  
409 dominating effect of aerosols is cooling corresponding to an overall negative forcing at the  
410 TOA. The latitudinal variations in the surface air temperature changes are consistent with the  
411 AOD distribution, with a maximum up to  $-0.45 \text{ K}$  at around  $26^\circ\text{N}$ . Of the three simulations,  
412 Case II estimates the largest cooling by aerosols at the surface, although the largest surface  
413 dimming of the incoming radiation is given by Case I (Table 3). This could be because  
414 aerosols over land are generally concentrated near the surface, and the aerosol-induced  
415 warming of the lower atmosphere offsets the cooling due to the surface dimming (Penner et  
416 al., 2003). Because Case I has more absorbing aerosols, the near-surface compensating  
417 heating effect is stronger, resulting in weaker surface cooling for the same AOD conditions as  
418 in Case II. The breakdown of the heating rate changes due to individual processes is  
419 discussed in the next section.

### 420 **3.4 Lower-atmosphere heating rate response**

421 In addition to instantaneous radiative heating due to aerosol absorption of solar radiation,  
422 rapid adjustments in the surface energy balance and BL dynamical and thermodynamical  
423 processes also influence the heating rate in the lower atmosphere. The heating rate in a  
424 volume of air or the temperature tendency term ( $dT/dt$ ) is calculated in the WRF-Chem model



425 as a function of altitude for five different physical processes: shortwave (SW) and longwave  
426 (LW) radiation, BL mixing, exchange of the latent heat flux in cloud microphysics (Micro),  
427 and heat transport in cumulus (deep convection) parameterization. The differences in the  
428 calculated heating rates with and without aerosols are shown in Fig. 4 for individual  
429 processes, except that cumulus cloud parameterization — a small term at a grid spacing of 12  
430 km in March — is not shown. The heating rate profiles are shown separately over the land  
431 (Figs. 4a-c) and oceans (Figs. 4d-f). The land-ocean contrast is evident in SW heating rates  
432 that are much more significant over land because of higher aerosol loadings. The SW heating  
433 over the ocean peaks at more elevated levels, mostly above  $\sim 900$  hPa, not as close to the  
434 surface as over the continental source regions. Since the sea surface temperature is fixed in  
435 the simulations, stronger lower-atmosphere thermodynamic responses (indicated by larger  
436 heating rates) are estimated over the land than over the ocean for BL and LW process.

437 Consistent with the atmospheric forcing shown in Table 3, Case I estimates the largest  
438 diurnal mean SW heating rate (maximum  $\sim 0.7$  K/day) of the three cases, and the SW heating  
439 rate in Case II is similar to that for the control run (maximum  $\sim 0.35$  K/day). Forced by the  
440 same aerosol extinction profiles with the bias correction, the differences in calculated heating  
441 rates for individual processes between Case I and Case II are shown in Fig. 4. These results  
442 demonstrate the impact of different absorbing aerosol profiles on boundary layer dynamics  
443 and cloud microphysics processes. The BL cooling is initiated as a dynamical response to  
444 both surface dimming (reduced sensible and latent heat fluxes) and atmospheric heating  
445 (enhanced or suppressed vertical mixing, depending on height). Over land, the local  
446 maximum cooling due to BL mixing occurs at the height with the largest SW heating; the  
447 larger SW heating in Case I also drives stronger BL cooling than in Case II. The LW radiation  
448 responds similarly to surface dimming and atmosphere heating, so Case I estimates the  
449 largest LW cooling over land. Over the ocean, the LW responses are also affected by cloud  
450 microphysics processes (i.e., the subsequent latent heat flux exchanges from cloud  
451 condensation and evaporation [Micro]). Because absorbing aerosols tend to stabilize the  
452 lower atmosphere and suppress the cloud formation, Case I estimates a smaller Micro heating  
453 rate at the cloud condensation level and also a smaller LW heating (cooling) below (above)  
454 the cloud layer over the ocean than Case II.

455 The total aerosol impact on the lower-atmosphere temperature profile is determined by  
456 the combined effects of all the heating rates (solid black line in Fig. 4). Over the ocean, the  
457 total heating rate is strongly governed by the SW heating. Thus, Case I calculates the most  
458 significant atmospheric heating by aerosols, which warms most of the lower atmosphere  
459 below 600 hPa. The maximum heating occurs below the level where the SW heating rate  
460 peaks, because of compensating LW cooling by lower marine clouds. The heating response is  
461 different over land. The calculated total heating rate deviates from the SW heating profile in  
462 the lower atmosphere as a result of rapid thermodynamic adjustments over the land surface  
463 and through BL mixing. Aerosols tend to have an overall cooling effect (negative heating rate)  
464 near the surface that exceeds the direct instantaneous SW radiative heating. The surface  
465 cooling rate is enhanced from  $\sim -0.4$  K/day in the control run to  $-0.7$  K/day in Case I and  $-0.8$   
466 K/day in Case II after aerosol extinctions are increased nearly to the observed levels.

467 Furthermore, sensitivity studies of unconstrained partitioning between absorbing and  
468 scattering components of aerosols (Case I versus Case II) show that higher atmospheric  
469 heating due to a larger absorption fraction (as in Case I) offsets part of the near-surface BL  
470 and LW cooling responses generated, which are similar to those in Case II. Therefore, Case I  
471 warms the lower atmosphere more pronouncedly than Case II but cools less at the land  
472 surface. This implies that the manifestation of aerosol direct and semi-direct radiative effects  
473 not only depends on the aerosol extinction profile but also is affected strongly by aerosol  
474 absorption. These uncertainties in the estimated heating rates resulting from aerosol vertical  
475 distributions further propagate into simulations of the BL height and cloudiness, as discussed  
476 below.

### 477 **3.5 Atmospheric dynamic and thermodynamic responses**

478 As a result of changes in the heating rate, aerosol effects tend to stabilize the lower  
479 atmosphere over land. As Fig. 5 shows, the predicted BL height is lowered over most of the  
480 land areas in all three simulations compared to the run without aerosol-radiation feedbacks.  
481 The reduction in the BL height is about  $-10\%$  to  $-20\%$  at locations where the estimated peak  
482 BL height (at 1300-1400 local time) is above 2-3 km during the pre-monsoon month. The  
483 aerosol impact on the BL height is more significant with increased AOD or extinction in the  
484 sensitivity studies, Case I and Case II, than in the control run. Moreover, more absorbing

485 aerosols in Case I result in smaller reductions in the BL height than in Case II. This implies  
486 that the BL height is predominately linked to surface cooling. Because Case II generates the  
487 largest cooling at the surface (Fig. 3), we obtain the largest reductions in the BL heights for  
488 Case II. On some portions of the ocean and land surfaces, the BL height is moderately higher  
489 (roughly about 200 m) with aerosols, and these regions correspond to areas where aerosols  
490 generally have a warming effect on the near-surface air temperature.

491 Figure 6 illustrates percent changes due to aerosols in meridional circulation ( $v$ ,  $-\omega$ ) and  
492 total precipitable water vapor (background color map) averaged at 60-95°E. These changes  
493 are linked closely to anomalies of total heating or cooling in the atmosphere (Fig. 4). At  
494 5-20°N where ocean prevails, atmospheric heating by aerosols results in strengthening of the  
495 upward motion in all three model simulations, especially below 700 hPa (Figs. 6a-c). This is  
496 accompanied by enhanced large-scale subsidence in the lower troposphere north of 20°N  
497 where land surface prevails and aerosols have an overall cooling effect due to strong negative  
498 LW and BL responses. The largest enhancement in the ascending zone for aerosols is in Case  
499 I, which also has the highest absorbing aerosol content. Similarly, Case II, with the strongest  
500 cooling, calculates the largest enhancement in the descending zone.

501 The changes in updraft and downdraft are consistent with the aerosol-induced changes in  
502 surface pressure, as illustrated in Fig. 6d for Case I. The decreased pressure over the ocean  
503 and an increase over the northern Indian subcontinent are accompanied by enhanced  
504 convergence at 850 hPa over the Arabian Sea and enhanced divergence over the eastern India  
505 coast, adjacent to the Bay of Bengal. The high-pressure system and divergence drive  
506 recirculation of the subsidence flow northward and form more terrain-elevated convection  
507 along the Himalayan foothills. Aerosols transported over high-elevation mountains induce a  
508 warming effect over the snow-covered surface by reducing the surface albedo, thus enhancing  
509 convective updraft over the Qinghai–Tibet Plateau.

510 In response to the radiative and dynamical perturbation, the aerosol-induced  
511 thermodynamic responses are manifested through enhanced surface evaporation and upward  
512 transport of clean, moist marine air from the northern Indian Ocean (Figs. 6a-c). The  
513 elevation of water vapor to the upper troposphere in the tropics leads to reduced moisture in  
514 the middle troposphere over the subtropics. The calculated percent changes in predicted total

515 precipitable water vapor are very sensitive to the aerosol properties simulated. Compared  
516 with the control run, Case I predicts both larger increases of water vapor at 5-20°N and larger  
517 decreases of water vapor north of 20°N in the free troposphere, as a result of increased  
518 aerosol extinctions and AOD. On the other hand, Case II has the same aerosol extinctions and  
519 AOD as Case I but gives rise to weaker BL moistening in the tropics and stronger drying (by  
520 about 50% drier than Case I) in the middle troposphere of the subtropics (>15°N), as a result  
521 of less light-absorptive aerosols.

522 As for water vapor, Fig. 7 shows responses in cloudiness for different aerosol simulations.  
523 Cloud frequency of occurrence is calculated as percent of hours in a month with non-zero  
524 liquid water cloud fraction below 500 hPa in each column. In pre-monsoonal March, clouds  
525 occur more frequently over the tropical and subtropical ocean than land, in the range of 20-80%  
526 (green contour lines in Fig. 7). Over most of the land, cloud occurrence is lower than 10%,  
527 except for the mountainous areas and over the Plateau with orographic and convective cloud  
528 formation which is either not very susceptible to aerosol effects or has low aerosol  
529 concentrations. Therefore, over the polluted land surface, in spite of high aerosol loadings,  
530 cloud changes resulting from the simulated aerosol effects are small within  $\pm 5\%$  and  
531 considered as insignificant, as shown by the color map in Fig. 7a. The most significant cloud  
532 response is found over the Bay of Bengal at 10-20°N, where the cloud occurrence exceeds 60%  
533 of the time and aerosol loadings are also high. Increased aerosol extinctions in Case I (Fig. 7b)  
534 and Case II (Fig. 7c) result in different cloud responses from the control run (Fig. 7a), which  
535 calculates a moderate increase of 5-10% in cloudiness due to aerosols. Case I enhances the  
536 aerosol effect in the control run and calculates a distinct and overwhelming increase of 10-20%  
537 more cloudy skies over this region, whereas cloud formation in Case II is largely suppressed  
538 and aerosols are found to decrease cloudiness by about 5-10% over some areas. Therefore,  
539 while aerosol extinctions being the same, a smaller SSA (more absorbing aerosols) in Case I  
540 could change the cloud response to aerosol radiative effects from negative to positive in  
541 pre-monsoon month. And this uncertainty in cloud response up to 10-20% could contribute to  
542 about one third of the calculated local cloud frequency of occurrence (40-60%).

#### 543 **4. Summary and Discussion**

544 Although aerosol radiative effects have been incorporated into global and regional

545 climate simulations, quantification of simulated aerosol vertical distributions and subsequent  
546 climate responses in large-scale models is lacking. This is of particular importance for  
547 climate studies over South Asia, where high concentrations of aerosols are possibly linked to  
548 weakening of the South Asian Monsoon in the 20th century (Bollasina et al., 2014). During  
549 March 2012, ground-based lidar measurements of vertical distributions of aerosol extinctions  
550 were made available in a polluted area of northern India, both at a high-elevation site  
551 (Nainital) near the BL top and at a valley site (Kanpur) near sea level. The aerosol extinction  
552 profiles retrieved at these two sites provide an independent ground calibration of CALIPSO  
553 satellite retrievals of aerosol vertical distributions, which cover a more extended domain.  
554 Together, the profiles are used to identify altitude-related bias in WRF-Chem regional model  
555 simulations of aerosol optical properties over this region.

556 Our study reveals some broad tendencies and biases in model AOD simulations over  
557 South Asia. Compared to the MODIS satellite AOD, the WRF-Chem model generally  
558 underestimates AOD, despite using a high-resolution regional model with a grid spacing of  
559 12 km and updated anthropogenic emissions. On a zonal or regional mean basis, the modeled  
560 AODs are underestimated by about half of the MODIS retrievals. Furthermore, we  
561 demonstrate that the low bias in column AOD is mainly associated with underprediction of  
562 aerosol extinctions in the lower troposphere versus observed extinction profiles. Systematic  
563 underestimation of > 50% was observed below 2-3 km at the two ground sites. Comparison  
564 with CALIPSO satellite data indicates even larger discrepancies of roughly 77% below ~2  
565 km on a regional mean basis, although some of the differences can be attributed to  
566 uncertainty associated with the CALIPSO retrievals of column AOD. Above ~2 km, the  
567 model's low bias in calculated aerosol extinction is smaller and the extent of the model  
568 underestimation also varies depending on the geographical locations. Previous studies have  
569 indicated similar low bias (to different extents) in modeled column AOD (Ganguly et al.,  
570 | 2009; Cherian et al., 2013; Pan et al., 2015<sup>4</sup>) and lower-atmosphere extinction coefficients  
571 (Yu et al., 2010; Koffi et al., 2012) over this region. Therefore, although the atmospheric  
572 radiative and dynamical responses derived from the sensitivity studies in this study are based  
573 on the WRF-Chem model used in this study, the dependence on aerosol extinction profiles  
574 might also be applicable to other model simulations.

575 Resolving the mismatch between simulated and observed aerosol extinction profiles  
576 requires possible upgrades of multiple model physics schemes and quantification of key  
577 parameters that could affect vertical distribution of aerosols, for instance, biomass burning  
578 injection heights (Grell et al., 2011), boundary layer height and near-surface winds (Nair et al.,  
579 2012) as well as a. Additionally, high-quality measurements at different locations are also  
580 needed for model evaluation over longer time periods, and it is recommended for future  
581 studies over this region. Here, instead of speculating on factors that contribute to the  
582 model-data differences, we apply a bias correction to simulated aerosol extinction profiles  
583 and demonstrate the impact on regional climate simulations. In our sensitivity studies,  
584 increases in aerosol extinction below 2-3 km lead to improved agreement in column AOD,  
585 from an underestimation of -66% to -11% relative to MODIS retrievals averaged over South  
586 Asia. This suggests that about 83% of the AOD underestimation is attributable to model  
587 levels below 2-3 km. In addition, the column-mean differences between modeled and  
588 CALIPSO extinction profiles averaged over the South Asia domain are reduced from 75% to  
589 40% or 16% if the CALIPSO profiles are normalized to the MODIS AOD retrievals. In the  
590 aerosol-concentrated lower atmosphere below 2-3 km, the predicted regional-mean extinction  
591 profile agrees with the CALIPSO retrieval within 30% or 0.4% compared with the CALIPSO  
592 profile normalized to the MODIS AOD.

593 Compared to the control run, the increased aerosol extinctions in Case I and Case II  
594 result in 63% and 80% larger negative forcing at the TOA for  $-4.9$  and  $-5.4 \text{ W m}^{-2}$ ,  
595 respectively, and 53% and 26% stronger dimming effects at the surface for  $-14.2$  and  $-11.7 \text{ W}$   
596  $\text{m}^{-2}$ , respectively. The contrast between Case I and Case II demonstrates the importance of  
597 constraining the vertical distribution of aerosol absorption, in addition to extinction profiles.  
598 When column AOD and extinction profiles are the same as in Case I and Case II, additional  
599 absorbing aerosols (a smaller SSA) in Case I generate a 48% larger atmospheric forcing for  
600  $+9.3 \text{ W m}^{-2}$ .

601 More importantly, we demonstrate that the larger atmospheric heating and surface  
602 dimming in Case I lead to smaller lower-atmosphere cooling (up to  $-0.7 \text{ K day}^{-1}$ ) over land  
603 than in Case II (up to  $-0.8 \text{ K day}^{-1}$ ); in the latter, the aerosols cause a smaller energy  
604 imbalance between the atmosphere and surface. This indicates that although absorbing

605 aerosols generate larger radiative heating in the atmosphere, they also cause stronger cooling  
606 responses from the land surface and BL. These rapid adjustments counteract atmospheric  
607 heating and lead to overall cooling at the surface and in the lower atmosphere. The resultant  
608 cooling effect is lower than that due to fewer absorbing aerosols with the same AOD (a larger  
609 SSA).

610 Consequently, atmospheric dynamic and thermodynamic processes also respond  
611 differently. Case I predicts smaller reductions in BL height than Case II over land, as a result  
612 of a more stabilized lower troposphere. On the other hand, the larger atmospheric warming  
613 due to increased absorption of solar radiation in Case I increases surface evaporation from the  
614 ocean and enhances the upward convective transport of moisture into the upper troposphere  
615 in the tropics. The consequence is a reduction in the transport of moisture to the subtropical  
616 lower-to-middle troposphere during the pre-monsoon time over this region. And clouds occur  
617 more frequently over the Bay of Bengal. Although the simulated aerosol perturbation is small  
618 for large-scale circulation (about 10 hPa day<sup>-1</sup> vertically, and 0.1 m s<sup>-1</sup> in the meridional  
619 direction), water vapor ( $\pm 6\%$ ), and cloud occurrence ( $\pm 10\%$ ), the propagated uncertainty due  
620 to aerosol extinction is comparable to the absolute aerosol effect, and the partitioning of  
621 absorbing and scattering aerosols could change the sign of these responses.

622 In this work, we had to limit the evaluation of model vertical extinction profiles to one  
623 month, because of the need for ground-based vertical profile observations at different  
624 locations and times to validate and supplement the CALIPSO satellite retrievals. It would be  
625 desirable to conduct similar evaluations for longer times [and use ensemble members of](#)  
626 [perturbed meteorological conditions](#) to better investigate the climate response to uncertainties  
627 in modeled aerosols. In addition, observational constraints on aerosol absorption profiles are  
628 lacking. In particular, light absorption by brown carbon aerosols from biomass burning,  
629 which are important aerosol sources in South Asia, might contribute additional aerosol  
630 absorption (Feng et al., 2013). This absorption enhancement is not considered in this version  
631 of the WRF-Chem model used for this study and evaluated. Also, model simulations of  
632 semi-direct aerosol effects depend strongly on the model representation of clouds, which is  
633 not examined here; on the other hand, cloud occurrences are generally low over this region  
634 during the pre-monsoon month.

635        Nevertheless, this study improves the understanding of model underestimation of  
636 aerosols in particular their vertical distribution over South Asia and highlights the importance  
637 of accurate representation of both aerosol extinction and absorption profiles in regional  
638 climate simulations. Determining whether aerosol scattering or absorption contributes to the  
639 aerosol optical underestimation is critical, because the two sensitivity studies here reveal  
640 different responses in predicted large-scale dynamics and in subsequent water vapor and  
641 cloud distributions. Additional high-quality, routine measurements of both aerosol extinction  
642 and absorption profiles are needed. Furthermore, we show that rapid adjustments in the land  
643 surface energy budget and atmospheric dynamics modulate the instantaneous radiative  
644 perturbation by aerosols with comparable force and can either amplify or offset the direct  
645 aerosol radiative forcing. Our results thus reinforce the need for observational constraints of  
646 effective radiative forcing, which includes both direct and semi-direct radiative effects, for  
647 quantifying aerosol-radiation interactions, as suggested in the Intergovernmental Panel on  
648 Climate Change fifth assessment report (Boucher et al., 2013).

649

650

651 **Acknowledgments.** This work was supported by the U.S. Department of Energy (DOE) as  
652 part of the Atmospheric System Research Program. Support for this research was provided to  
653 YF, VRK, RC, and MC by Argonne National Laboratory under U.S. DOE contract  
654 DE-AC02-06CH11357. CZ's contribution to this study was supported by the U.S. DOE as  
655 part of the Regional and Global Climate Modeling program through contract  
656 DE-AC05-76RL01830. All of the numerical simulations were performed by using the  
657 computing cluster (Fusion) operated by the Argonne's Laboratory Computing Resource  
658 Center.

659



660 **References**

661

662 Ban-Weiss, G., L. Cao, G. Bala, and K. Caldeira: Dependence of climate forcing and  
663 response on the altitude of black carbon aerosols. *Clim. Dyn.*, 38, 897–911, 2012.

664 Benjamin, S. G., G. A. Grell, J. M. Brown, and T. G. Smirnova: Mesoscale weather prediction  
665 with the RUC hybrid isentropic-terrain-following coordinate model. *Mon. Wea. Rev.*, 132,  
666 473-494, 2004.

667 Bollasina, M. A., Y. Ming, and V. Ramaswamy: Anthropogenic aerosols and the weakening of  
668 the South Asian summer monsoon, *Science*, 334(6055), 502–505,  
669 doi:10.1126/science.1204994, 2011.

670 Bollasina, M. A., Y. Ming, V. Ramaswamy, M. D. Schwarzkopf, and V. Naik: Contribution of  
671 local and remote anthropogenic aerosols to the twentieth century weakening of the South  
672 Asian Monsoon, *Geophys. Res. Lett.*, 41, 680–687, doi:10.1002/2013GL058183, 2014.

673 Boucher, O., D. Randall, P. Artaxo, C. Bretherton, G. Feingold, P. Forster, V.-M. Kerminen, Y.  
674 Kondo, H. Liao, U. Lohmann, P. Rasch, S.K. Satheesh, S. Sherwood, B. Stevens and X.Y.  
675 Zhang, Clouds and Aerosols. In: *Climate Change 2013: The Physical Science Basis.*  
676 *Contribution of Working Group I to the Fifth Assessment Report of the*  
677 *Intergovernmental Panel on Climate Change* [Stocker, T.F., D. Qin, G.-K. Plattner, M.  
678 Tignor, S.K. Allen, J. Boschung, A. Nauels, Y. Xia, V. Bex and P.M. Midgley (eds.)].  
679 Cambridge University Press, Cambridge, United Kingdom and New York, NY, USA,  
680 2013.

681 Cherian, R., C. Venkataraman, J. Quaas, and S. Ramachandran: GCM simulations of  
682 anthropogenic aerosol-induced changes in aerosol extinction, atmospheric heating and  
683 precipitation over India, *J. Geophys. Res. Atmos.*, 118, 2938–2955,  
684 doi:10.1002/jgrd.50298, 2013.

685 Chin, M., Ginoux, P., Kinne, S., Holben, B. N., Duncan, B. N., Martin, R. V., Logan, J. A.,  
686 Higurashi, A., and Nakajima, T.: Tropospheric aerosol optical thickness from the  
687 GOCART model and comparisons with satellite and sunphotometer measurements, *J.*  
688 *Atmos. Sci.*, 59, 461–483, 2002.

689 Choi, J.-O., and C. E. Chung: Sensitivity of aerosol direct radiative forcing to aerosol vertical

690 profile, *Tellus B*, 66, 24376, <http://dx.doi.org/10.3402/tellusb.v66.24376>, 2014.

691 Chung, C. E., Ramanathan, V., Carmichael, G., Kulkarni, S., Tang, Y., Adhikary, B.,  
692 Leung, L. R., and Qian, Y.: Anthropogenic aerosol radiative forcing in Asia derived from  
693 regional models with atmospheric and aerosol data assimilation, *Atmos. Chem. Phys.*, 10,  
694 6007-6024, doi:10.5194/acp-10-6007-2010, 2010.

695 Dey, S., and L. Di Girolamo: A climatology of aerosol optical and microphysical properties  
696 over the Indian subcontinent from nine years (2000–2008) of Multiangle Imaging  
697 SpectroRadiometer (MISR) data, *J. Geophys. Res.*, 115, D15204,  
698 doi:10.1029/2009JD013395, 2010.

699 Eck, T. F., B. N. Holben, J. S. Reid, O. Dubovik, A. Smirnov, N. T. O’Neill, I. Slutsker, and S.  
700 Kinne: Wavelength dependence of the optical depth of biomass burning, urban, and  
701 desert dust aerosols, *J. Geophys. Res.*, 104, 31,333–31,349, doi:10.1029/1999JD900923,  
702 1999.

703 Emmons, L. K., Walters, S., Hess, P. G., Lamarque, J.-F., Pfister, G. G., Fillmore, D., Granier,  
704 C., Guenther, A., Kinnison, D., Laepple, T., Orlando, J., Tie, X., Tyndall, G., Wiedinmyer,  
705 C., Baughcum, S. L., and Kloster, S.: Description and evaluation of the Model for Ozone  
706 and Related chemical Tracers, version 4 (MOZART-4), *Geosci. Model Dev.*, 3, 43–67,  
707 doi:10.5194/gmd-3-43-2010, 2010.

708 Fast, J. D, Gustafson Jr., W. I., Easter, R. C., Zaveri, R. A., Barnard, J. C., Chapman, E. G.,  
709 and Grell, G. A.: Evolution of ozone, particulates, and aerosol direct forcing in an urban  
710 area using a new fully-coupled meteorology, chemistry, and aerosol model, *J. Geophys.*  
711 *Res.*, 111, D21305, doi:10.1029/2005JD006721, 2006.

712 Feng, Y., V. Ramanathan, and V. R. Kotamarthi, Brown Carbon: a Significant Atmospheric  
713 Absorber of Solar Radiation? *Atmos. Chem. Phys. Discuss.*, 13, 2795-2833,  
714 doi:10.5194/acpd-13-2795-2013, 2013.

715 Ganguly, D., P. Ginoux, V. Ramaswamy, D. M. Winker, B. N. Holben, and S. N. Tripathi:  
716 Retrieving the composition and concentration of aerosols over the Indo-Gangetic basin  
717 using CALIOP and AERONET data, *Geophys. Res. Lett.*, 36, L13806, doi:10.1029/  
718 2009GL038315, 2009.

719 Ganguly, D., Rasch, P. J., Wang, H., and Yoon, J.: Climate response of the South Asian

720 monsoon system to anthropogenic aerosols, *J. Geophys. Res.*, 117, D13209, 15  
721 doi:10.1029/2012JD017508, 2012.

722 Gautam, R., Hsu, N. C., and Lau, K.-M.: Premonsoon aerosol characterization and radiative  
723 effects over the Indo-Gangetic Plains: Implications for regional climate warming, *J.*  
724 *Geophys. Res.*, 115, D17208, doi:10.1029/2010JD013819, 2010.

725 Ginoux, P., Chin, M., Tegen, I., Prospero, J. M., Holben, B., Dubovik, O., and Lin, S. J.:  
726 Sources and distributions of dust aerosols simulated with the GOCART model, *J.*  
727 *Geophys. Res.- Atmos.*, 106, 20255–20273, 2001.

728 Grell, G. A., Peckham, S. E., Schmitz, R., McKeen, S. A., Frost, G., Skamarock, W. C., and  
729 Eder, B.: Fully coupled “online” chemistry within the WRF model, *Atmos. Environ.*, 39,  
730 6957–6975, 2005.

731 [Grell, G., Freitas, S. R., Stuefer, M., and Fast, J.: Inclusion of biomass burning in WRF-Chem:  
732 \[impact of wildfires on weather forecasts, \\*Atmos. Chem. Phys.\\*, 11, 5289-5303, 2011.\]\(#\)](#)

733 Haywood, J. M. and Shine, K. P.: Multi-spectral calculations of the direct radiative forcing of  
734 tropospheric sulphate and soot aerosols using a column model. *Q. J. Roy. Meteorol. Soc.*,  
735 123, 1907-1930, 1997.

736 Holben, B. N., Eck, T. F., Slutsker, I., et al.: AERONET – A federated instrument network and  
737 data archive for aerosol characterization, *Rem. Sens. Environ.*, 66, 1–16, 1998.

738 Iacono, M. J., J. S. Delamere, E. J. Mlawer, M. W. Shephard, S. A. Clough, and W. D. Collins:  
739 Radiative forcing by long-lived greenhouse gases: Calculations with the AER radiative  
740 transfer models. *J. Geophys. Res.*, 113, D13103, 2008.

741 Jacob, D. J., Crawford, J. H., Maring, H., Clarke, A. D., Dibb, J. E., Emmons, L. K., Ferrare,  
742 R. A., Hostetler, C. A., Russell, P. B., Singh, H. B., Thompson, A. M., Shaw, G. E.,  
743 McCauley, E., Pederson, J. R., and Fisher, J. A.: The Arctic Research of the Composition  
744 of the Troposphere from Aircraft and Satellites (ARCTAS) mission: design, execution,  
745 and first results, *Atmos. Chem. Phys.*, 10, 5191–5212, doi:10.5194/acp-10-5191-2010,  
746 2010.

747 Janjic, Z. I.: The Step–Mountain Eta Coordinate Model: Further developments of the  
748 convection, viscous sublayer, and turbulence closure schemes. *Mon. Wea. Rev.*, 122,  
749 927–945, 1994.

750 Kafle, D. N. and R. L. Coulter: Micropulse Lidar Derived Aerosol Optical Depth  
751 Climatology at ARM Sites Worldwide, *J. Geophys. Res.*, 118, 13, 7293-7308, doi:  
752 10.1002/jgrd.50536, 2013.

753 Kinne, S., et al.: An AeroCom initial assessment: optical properties in aerosol component  
754 modules of global models. *Atmos. Chem. Phys.* 6, 1815–1834, 2006.

755 Klett, J. D.: Stable analytical inversion solution for processing lidar returns. *Applied Optics*,  
756 Vol. 20, No. 2, pp211-220, Jan., 1981.

757 Koch, D., et al.: Evaluation of black carbon estimations in global aerosol models. *Atmos.*  
758 *Chem. Phys.*, 9, 9001–9026, 2009.

759 Koffi, B., Schulz, M., Breon, F. M., Griesfeller, J., Winker, D., Balkanski, Y., Bauer, S.,  
760 Berntsen, T., Chin, M. A., Collins, W. D., Dentener, F., Diehl, T., Easter, R., Ghan, S.,  
761 Ginoux, P., Gong, S. L., Horowitz, L. W., Iversen, T., Kirkevåg, A., Koch, D., Krol, M.,  
762 Myhre, G., Stier, P., and Takemura, T.: Application of the CALIOP layer product to  
763 evaluate the vertical distribution of aerosols estimated by global models: Aero-Com  
764 phase I results, *J. Geophys. Res.-Atmos.*, 117, D10201, doi:10.1029/2011jd016858, 2012.

765 Kuhlmann, J. and Quaas, J.: How can aerosols affect the Asian summer monsoon?  
766 Assessment during three consecutive pre-monsoon seasons from CALIPSO satellite data,  
767 *Atmos. Chem. Phys.*, 10, 4673-4688, doi:10.5194/acp-10-4673-2010, 2010.

768 Kumar, R., Barth, M. C., Pfister, G. G., Naja, M., and Brasseur, G. P.: WRF-Chem  
769 simulations of a typical pre-monsoon dust storm in northern India: influences on aerosol  
770 optical properties and radiation budget, *Atmos. Chem. Phys.*, 14, 2431-2446,  
771 doi:10.5194/acp-14-2431-2014, 2014.

772 Lau, K. M., M. K. Kim, and K. M. Kim: Asian summer monsoon anomalies induced by  
773 aerosol direct forcing: the role of the Tibetan Plateau, *Clim. Dyn.*, 26, 855-864, 2006.

774 Lau, K.-M., K.-M. Kim, C. N. Hsu, and B. N. Holben: Possible influences of air pollution,  
775 dust- and sandstorms on the Indian monsoon, *WMO Bull.*, 58, 22–30, 2009.

776 Liao, H. and Seinfeld, J. H.: Effects of clouds on direct aerosol radiative forcing of climate, *J.*  
777 *Geophys. Res.*, 103, 3781–3788, 1998.

778 Liu, X., et al.: Toward a minimal representation of aerosols in climate models: description  
779 and evaluation in the Community Atmosphere Model CAM5, *Geosci. Model. Dev.*, 5,

780 709–739, 2012.

781 Loeb, N. G., and W. Y. Su: Direct aerosol radiative forcing uncertainty based on a radiative  
782 perturbation analysis. *J. Clim.*, 23, 5288–5293, 2010.

783 Lohmann, U., and J. Feichter, Can the direct and semi-direct aerosol effect compete with the  
784 indirect effect on a global scale? *Geophys. Res. Lett.*, 28, 159–161, 2001.

785 Lu Z, Zhang, Q. and Streets D. G.: Sulfur dioxide and primary carbonaceous aerosol  
786 emissions in China and India 1996–2010, *Atmos. Chem. Phys.* 11 9839–9, 2011.

787 McComiskey, A., S. Schwartz, B. Schmid, H. Guan, E. Lewis, P. Ricchiazzi, and J. Ogren,  
788 Direct aerosol forcing: Calculation from observables and sensitivities to inputs. *J.*  
789 *Geophys. Res.*, 113, D09202, 2008.

790 Meehl, G. A., J. M. Arblaster, and W. D. Collins: Effects of black carbon aerosols on the  
791 Indian monsoon, *J. Clim.*, 21, 2869–2882, doi:10.1175/2008JCLI2362.1, 2008.

792 Misra, A., S. N. Tripathi, D. S. Kaul, and E. J. Welton: Study of MPLNET-Derived Aerosol  
793 Climatology over Kanpur, India, and Validation of CALIPSO Level 2 Version 3  
794 Backscatter and Extinction Products. *J. Atmos. Oceanic Technol.*, 29, 1285–1294, 2012.

795 Moorthy, K. K., S. S. Babu, M. R. Manoj, and S. K. Satheesh: Buildup of aerosols over the  
796 Indian Region, *Geophys. Res. Lett.*, 40, 1011–1014, doi:10.1002/grl.50165, 2013.

797 Myhre, G., Berglen, T. F., Johnsrud, M., Hoyle, C. R., Berntsen, T. K., Christopher, S. A.,  
798 Fahey, D. W., Isaksen, I. S. A., Jones, T. A., Kahn, R. A., Loeb, N., Quinn, P., Remer, L.,  
799 Schwarz, J. P., and Yttri, K. E.: Modelled radiative forcing of the direct aerosol effect  
800 with multi-observation evaluation, *Atmos. Chem. Phys.*, 9, 1365–1392,  
801 doi:10.5194/acp-9-1365-2009, 2009.

802 Myhre, G., et al.: Radiative forcing of the direct aerosol effect from AeroCom Phase II  
803 simulations. *Atmos. Chem. Phys.*, 13, 1853–1877, 2013.

804 Nair, V. S., Solmon, F., Giorgi, F., Mariotti, L., Babu, S. S., and Moorthy, K. K.: Simulation  
805 of South Asian aerosols for regional climate studies, *J. Geophys. Res.*, 117, D04209,  
806 doi:10.1029/2011JD016711, 2012.

807 ~~Pan, X., Chin, M., Gautam, R., Bian, H., Kim, D., Colarco, P. R., Diehl, T. L., Takemura, T.,~~  
808 ~~Pozzoli, L., Tsigaridis, K., Bauer, S., and Bellouin, N.: A multi-model evaluation of~~  
809 ~~aerosols over South Asia: Common problems and possible causes, *Atmos. Chem. Phys.*~~

810 [Discuss., 14, 19095–19147, doi:10.5194/acpd-14-19095-2014, 2014.](#)

811 [Pan, X., Chin, M., Gautam, R., Bian, H., Kim, D., Colarco, P. R., Diehl, T. L., Takemura, T.,](#)  
812 [Pozzoli, L., Tsigaridis, K., Bauer, S., and Bellouin, N.: A multi-model evaluation of](#)  
813 [aerosols over South Asia: common problems and possible causes, \*Atmos. Chem. Phys.\*,](#)  
814 [15, 5903-5928, doi:10.5194/acp-15-5903-2015, 2015.](#)

815 Penner, J.E., S.Y. Zhang, and C.C. Chuang: Soot and smoke aerosol may not warm climate. *J.*  
816 *Geophys. Res.*, 108(D21), 4657, doi:10.1029/2003JD003409, 2003.

817 Petters, M. D. and Kreidenweis, S. M.: A single parameter representation of hygroscopic  
818 growth and cloud condensation nucleus activity, *Atmos. Chem. Phys.*, 7, 1961-1971,  
819 doi:10.5194/acp-7-1961-2007, 2007.

820 Pfister, G. G., Parrish, D. D., Worden, H., Emmons, L. K., Edwards, D. P., Wiedinmyer, C.,  
821 Diskin, G. S., Huey, G., Oltmans, S. J., Thouret, V., Weinheimer, A., and Wisthaler, A.:  
822 Characterizing summertime chemical boundary conditions for air masses entering the US  
823 West Coast, *Atmos. Chem. Phys.*, 11, 1769–1790, doi:10.5194/acp-11-1769-2011, 2011.

824 Platnick, S., King, M. D., Ackerman, S. A., Menzel, W. P., Baum, B. A. and co-authors:  
825 TheMODIS cloud products: algorithms and examples from Terra. *IEEE T Geosci.*  
826 *Remote*, 41, 2, 459–473, 2003.

827 [Quennehen, B., Raut, J.-C., Law, K. S., Ancellet, G., Clerbaux, C., Kim, S.-W., Lund, M. T.,](#)  
828 [Myhre, G., Olivié, D. J. L., Safieddine, S., Skeie, R. B., Thomas, J. L., Tsyro, S.,](#)  
829 [Bazureau, A., Bellouin, N., Daskalakis, N., Hu, M., Kanakidou, M., Klimont, Z.,](#)  
830 [Kupiainen, K., Myriokefalitakis, S., Quaas, J., Rumbold, S. T., Schulz, M., Cherian, R.,](#)  
831 [Shimizu, A., Wang, J., Yoon, S.-C., and Zhu, T.: Multi-model evaluation of short-lived](#)  
832 [pollutant distributions over East Asia during summer 2008, \*Atmos. Chem. Phys. Discuss.\*,](#)  
833 [15, 11049-11109, doi:10.5194/acpd-15-11049-2015, 2015.](#)

834 Ramana, M. V., Ramanathan, V., Kim, D., Roberts, G. C., and Corrigan, C. E.: Albedo:  
835 Atmospheric solar absorption and heating rate measurements with stacked UAVs, *Q. J.*  
836 *Roy. Meteor. Soc.*, 133, 1913–1931, 2007.

837 Ramanathan, V., C. Chung, D. Kim, T. Bettge, L. Buja, J. T. Kiehl, W. M. Washington, Q. Fu,  
838 D. R. Sikka, and M. Wild: Atmospheric brown clouds: Impacts on South Asian climate  
839 and hydrological cycle, *P Natl Acad Sci USA*, 102(15), 5326-5333, 2005.

840 Ramanathan, V., et al.: Indian Ocean experiment: An integrated analysis of the climate  
841 forcing and effects of the great Indo-Asian haze. *J. Geophys. Res.*, 106(D22), 28371–  
842 28398, 2001

843 Ramanathan, V., M. V. Ramana, G. Roberts, D. Kim, C. Corrigan, C. Chung, and D. Winker:  
844 Warming trends in Asia amplified by brown cloud solar absorption, *Nature*, 448, 575-578,  
845 doi:10.1038/nature06019, 2007.

846 Samset, B. H., et al.: Black carbon vertical profiles strongly affect its radiative forcing  
847 uncertainty, *Atmos. Chem. Phys.*, 13, 2423–2434, 2013.

848 Satheesh, S. K., K. K. Moorthy, S. S. Babu, V. Vinoj, and C. B. S. Dutt: Climate implications  
849 of large warming by elevated aerosol over India, *Geophys. Res. Lett.*, 35, L19809,  
850 doi:10.1029/2008GL034944, 2008.

851 Satheesh, S. K., K. K. Moorthy, S. S. Babu, V. Vinoj, V. S. Nair, S. N. Beegum, C. B. S. Dutt,  
852 D. P. Alappattu, and P. K. Kunhikrishnan: Vertical structure and horizontal gradients of  
853 aerosol extinction coefficients over coastal India inferred from airborne lidar  
854 measurements during the Integrated Campaign for Aerosol, Gases and Radiation Budget  
855 (ICARB) field campaign, *J. Geophys. Res.*, 114, D05204, doi:10.1029/2008JD011033,  
856 2009.

857 Schmid, B., J. Michalsky, R. Halthore, M. Beauharnois, L. Harrison, J. Livingston, P. Russell,  
858 B. Holben, T. Eck, and A. Smirnov: Comparison of aerosol optical depth from four solar  
859 radiometers during the fall 1997 ARM intensive observation period, *Geophys. Res. Lett.*,  
860 26, 2725 – 2728, doi:10.1029/1999GL900513, 1999.

861 Schwarz, J. P., et al.: Global-scale black carbon profiles observed in the remote atmosphere  
862 and compared to models. *Geophys. Res. Lett.*, 37, L18812, 2010.

863 Shindell, D.T., J.-F. Lamarque, M. Schulz, M. Flanner, C. Jiao, M. Chin, P.J. Young, Y.H. Lee,  
864 L. Rotstayn, N. Mahowald, G. Milly, G. Faluvegi, Y. Balkanski, W.J. Collins, A.J.  
865 Conley, S. Dalsoren, R. Easter, S. Ghan, L. Horowitz, X. Liu, G. Myhre, T. Nagashima,  
866 V. Naik, S.T. Rumbold, R. Skeie, K. Sudo, S. Szopa, T. Takemura, A. Voulgarakis, J.-H.  
867 Yoon, and F. Lo: Radiative forcing in the ACCMIP historical and future climate  
868 simulations. *Atmos. Chem. Phys.*, 13, 2939-2974, doi:10.5194/acp-13-2939-2013, 2013.

869 Skamarock, W. C., Klemp, J. B., Dudhia, J., Gill, D. O., Barker, D. M., Wang, W., and Powers,

870 J. G.: A description of the advancedresearch WRF version 2, NCAR Tech. Note,  
871 NCAR/TN- 468+STR, Natl. Cent. for Atmos. Res., Boulder, Colo, available at:  
872 <http://wrf-model.org/wrfadmin/publications.php>, 2008.

873 Smirnov, A., B. N. Holben, T. F. Eck, O. Dubovik, and I. Slutsker: Cloud screening and  
874 quality control algorithms for the AERONET data base, *Remote Sens. Environ.*, 73, 337–  
875 349, 2000.

876 Thompson, G., P. R. Field, R. M. Rasmussen, and W. D. Hall: Explicit Forecasts of Winter  
877 Precipitation Using an Improved Bulk Microphysics Scheme. Part II: Implementation of  
878 a New Snow Parameterization, *Mon. Wea. Rev.*, 136, 5095–5115, 2008.

879 Vuolo, M. R., Schulz, M., Balkanski, Y., and Takemura, T.: A new method for evaluating the  
880 impact of vertical distribution on aerosol radiative forcing in general circulation models,  
881 *Atmos. Chem. Phys.*, 14, 877-897, doi:10.5194/acp-14-877-2014, 2014.

882 Wang, C., D. Kim, A. M. L. Ekman, M. C. Barth, and P. J. Rasch: Impact of anthropogenic  
883 aerosols on Indian summer monsoon, *Geophys. Res. Lett.*, 36, L21704,  
884 doi:10.1029/2009GL040114, 2009.

885 Welton, E. J., and J. R. Campbell: Micropulse lidar signals: Uncertainty analysis. *J. Atmos.*  
886 *Oceanic Technol.*, 19, 2089–2094, 2002.

887 Welton, E. J., J. R. Campbell, J. D. Spinhirne, and V. S. Scott III: Global monitoring of clouds  
888 and aerosols using a network of micropulse lidar systems. *Lidar Remote Sensing for*  
889 *Industry and Environment Monitoring*, U. N. Singh, Ed., International Society for  
890 Optical Engineering (SPIE Proceedings, Vol. 4153), 151–158, doi:10.1117/12.417040,  
891 2001.

892 Winker, D. M., Vaughan, M. A., Omar, A. H., Hu, Y., Powell, K. A., Liu, Z., Hunt, W. H., and  
893 Young, S. A.: Overview of the CALIPSO Mission and CALIOP Data Processing  
894 Algorithms, *J. Atmos. Oceanic Technol.*, 26, 2310–2323, 2009.

895 Yevich, R., and J. A. Logan: An assessment of biofuel use and burning of agricultural waste  
896 in the developing world, *Global Biogeochem. Cycles*, 17(4), 1095,  
897 doi:10.1029/2002GB001952, 2003.

898 Yu, H. B., M. Chin, D. M. Winker, A. H. Omar, Z. Y. Liu, C. Kittaka, and T. Diehl: Global  
899 view of aerosol vertical distributions from CALIPSO lidar measurements and GOCART



900 simulations: Regional and seasonal variations. *J. Geophys. Res.*, 115, D00H30, 2010.

901 Yu, H., R. E. Dickinson, M. Chin, Y. J. Kaufman, B. N. Holben, I. V. Geogdzhayev, and M. I.  
902 Mishchenko: Annual cycle of global distributions of aerosol optical depth from  
903 integration of MODIS retrievals and GOCART model simulations, *J. Geophys. Res.*,  
904 108(D3), 4128, doi:10.1029/2002JD002717, 2003.

905 Zarzycki, C. M. and Bond, T. C.: How much can the vertical distribution of black carbon  
906 affect its global direct radiative forcing? *Geophys. Res. Lett.*, 37, L20807,  
907 doi:10.1029/2010gl044555, 2010.

908 Zhang, G. J., and N. A. McFarlane: Sensitivity of climate simulations to the parameterization  
909 of cumulus convection in the Canadian Climate Centre general circulation model.  
910 *Atmos.– Ocean*, 33, 407–446, 1995.

911 Zhao, C., X. Liu, L. L. Ruby, and S. Hagos: Radiative impact of mineral dust on monsoon  
912 precipitation variability over West Africa, *Atmos. Chem. Phys.*, 11:1879–1893, 2011.

913 

---

914

915 **Tables**916 **Table 1.** Estimated differences relative to CALIPSO extinction profiles at Nainital, Kanpur,  
917 and South Asia in March 2012

Site	Column Differences (%)			Differences below 850 hPa (%)		
	Model (control run)	Model (increased extinction)	Model (increased extinction)*	Model (control run)	Model (increased extinction)	Model (increased extinction)*
Nainital	-33	-22	-25	-56	-12	-16
Kanpur	-33	-14	-33	-52	-11	-31
S. Asia	-75	-40	-16	-77	-30	-0.4

918 \*Percent differences relative to the CALIPSO extinction profiles normalized to the column  
919 AOD inferred from the surface measurements for Nainital and Kanpur and the MODIS data  
920 for South Asia.

921

922

923 **Table 2.** Calculated mean extinction height (km) from observations (MPL and CALIPSO)  
924 and model simulations over different regions in March 2012

	Calculated Mean Extinction Height (km)					
	Nainital	Kanpur	Indo-Ganges basin	Central India	North Indian Ocean	South Asia
MPL	4.11	1.39	-	-	-	-
CALIPSO*	3.55 (3)	1.48 (4)	1.53 (9)	1.74 (4)	1.09 (5)	1.70 (29)
Model (control run)	4.00	2.09	1.86	1.91	1.73	1.85
Model (increased extinction)	3.64	1.68	1.69	1.68	1.53	1.68

925 \*Numbers in the parentheses are the counts of CALIPSO tracks of the month.

926

927 **Table 3.** Aerosol-induced changes in shortwave radiation flux calculated by the WRF-Chem  
928 model in the control run and two sensitivity studies (Case I and Case II) for March 2012,  
929 averaged for 60-95°E, and 0-36°N.

	Aerosol-Induced Change ( $W m^{-2}$ )		
	Control run	Case I	Case II
Top of the atmosphere	-3.0	-4.9	-5.4
Atmosphere	+6.3	+9.3	+6.3
Surface	-9.3	-14.2	-11.7

930

931

932

933 **Figures**

934 **Figure 1.** For March 2012: (a) MODIS-retrieved and (b) simulated monthly mean AOD  
935 distributions over South Asia. The locations of Nainital and Kanpur sites are indicated by red  
936 dots. (c) Latitudinal variations in AOD averaged for 60-95°E from the model control run (red  
937 solid), sensitivity runs (red dotted dash), and MODIS retrievals (blue). North of 27°N, more  
938 than 2/3 of the MODIS AODs are missing (data not shown). (d) Comparison of simulated and  
939 observed daily mean AOD at Nainital and Kanpur

940 **Figure 2.** Comparisons of monthly mean aerosol extinction profiles from model calculations  
941 at 550nm (red squares for the control run and green open circles for the sensitivity studies),  
942 ground-based MPL data at 532nm (solid black), satellite-retrieved CALIPSO data at 532nm  
943 (dashed black), and CALIPSO data normalized to the MODIS AODs (dashed blue) (a) at  
944 Nainital, (b) at Kanpur, and (c) over South Asia (60-95°E, 0-30°N), respectively. The  
945 column-mean uncertainty in CALIPSO extinction data is  $\pm 110\%$ ,  $\pm 93\%$ , and  $\pm 91\%$  in panels  
946 (a)-(c); Percent differences between the simulated and CALIPSO profiles are shown for (d)  
947 Nainital, (e) Kanpur, and (f) South Asia

948 **Figure 3.** Changes in surface air temperature (K) due to aerosol radiative effects for three  
949 model simulations

950 **Figure 4.** Calculated monthly mean heating rates (temperature tendency,  $dT/dt$ , in K/day)  
951 perturbed by aerosols, over land for (a) the control run, (b) Case I, and (c) Case II, as well as  
952 over the ocean for (d) the control run, (e) Case I, and (f) Case II. The heating processes  
953 include shortwave (SW) radiation (red), longwave (LW) radiation (blue dashed), boundary  
954 mixing (BL; magenta dashed), and cloud microphysics (Micro; green). The total heating due  
955 to aerosol effects is shown with solid black lines

956 **Figure 5.** (a) Calculated monthly mean planetary BL height (PBLH) at 1300-1400 local time  
957 for March, without aerosols; and estimated changes in PBLH ( $\Delta PBLH$ ) due to aerosols in (b)  
958 the control run, (c) Case I, and (d) Case II

959 **Figure 6.** Changes in meridional circulation ( $v$ ,  $-\omega$ ), averaged at  $60-95^\circ\text{E}$ , due to different  
960 aerosol effects for (a) the control run, (b) Case I, and (c) Case II, where  $v$  (scaled to  $0.1\text{ m/s}$ )  
961 is the meridional velocity, and  $-\omega$  (scaled to  $10\text{ hPa/day}$ ) is the vertical velocity. The  
962 color-shaded contours in the background indicate the changes (%) in total precipitable water  
963 ( $\Delta Q_v$ ) in the column due to aerosols. Panel (d) shows the changes in horizontal winds ( $u$ ,  $v$ )  
964 at  $850\text{ hPa}$  and surface pressure changes ( $\Delta\text{PSURF}$ ) due to aerosols for Case I

965 **Figure 7.** Changes in frequency of cloud occurrence (defined as % of hours in a month with  
966 clouds below  $500\text{hPa}$  in each column) due to aerosols for (a) the control run, (b) Case I, and  
967 (c) Case II. The contour lines in green color in each panel indicate calculated frequency of  
968 cloud occurrence without aerosols. The contour levels are shown for 10%, 20%, 40%, and  
969 60%

970

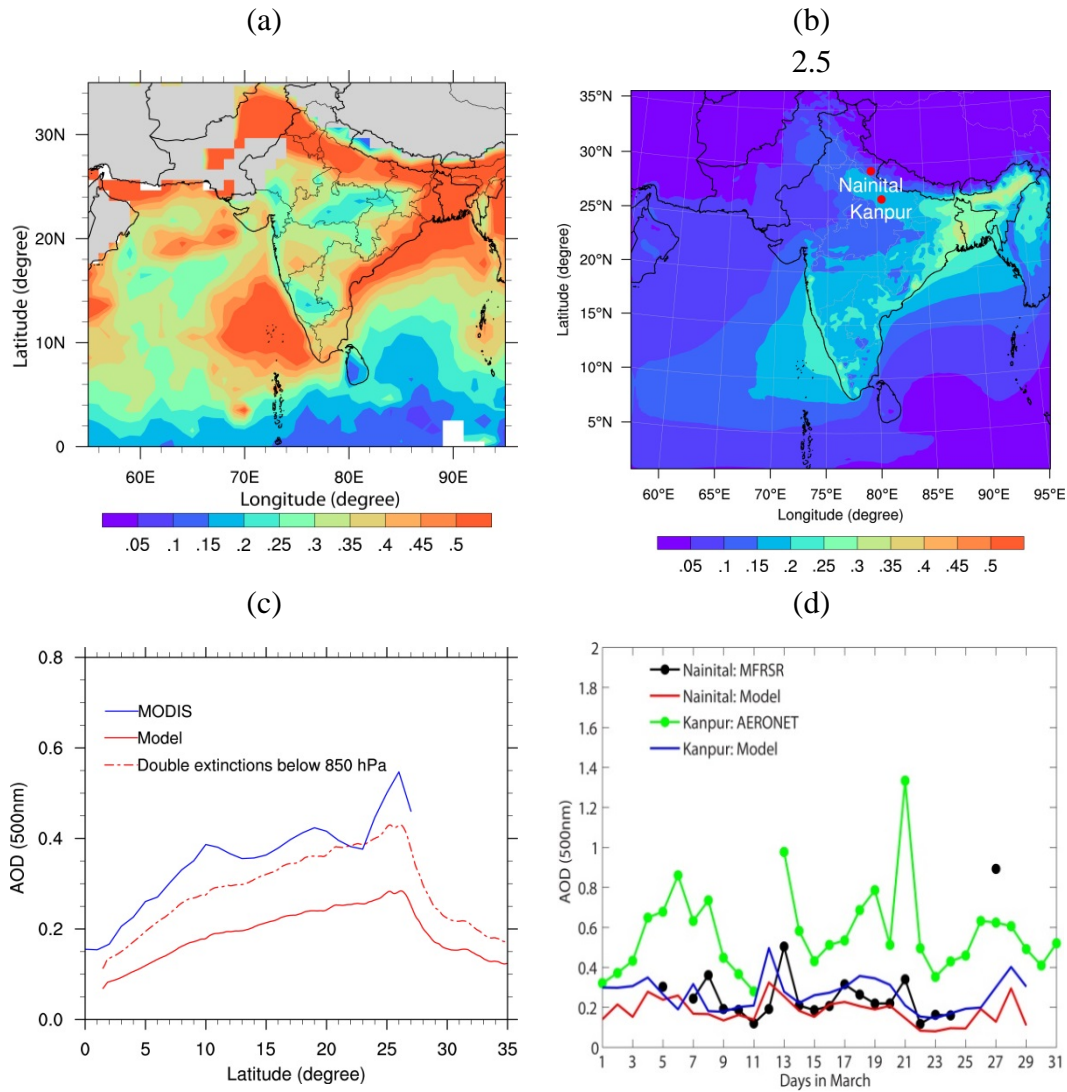


**Figure 1.** For March 2012: (a) MODIS-retrieved and (b) simulated monthly mean AOD distributions over South Asia. The locations of Nainital and Kanpur sites are indicated by red dots. (c) Latitudinal variations in AOD averaged for 60-95°E from the model control run (red solid), sensitivity run (red dotted dash), and MODIS retrievals (blue). North of 27°N, more than 2/3 of the MODIS AODs are missing (data not shown). (d) Comparison of simulated and observed daily mean AOD at Nainital and Kanpur

971

972

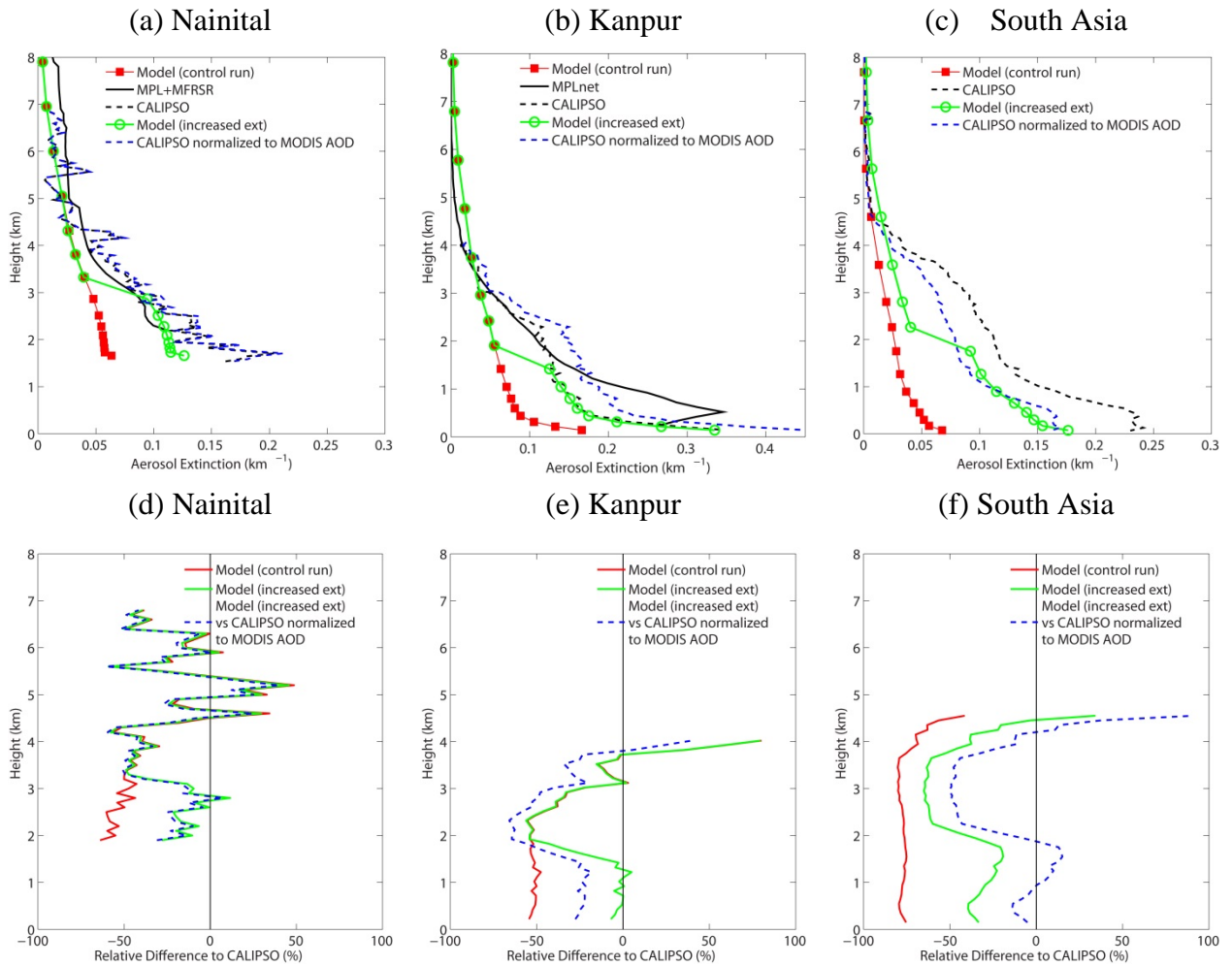


**Figure 2.** Comparisons of monthly mean aerosol extinction profiles from model calculations at 550nm (red squares for the control run and green open circles for the sensitivity studies), ground-based MPL data at 532nm (solid black), satellite-retrieved CALIPSO data at 532nm (dashed black), and CALIPSO data normalized to the MODIS AODs (dashed blue) (a) at Nainital, (b) at Kanpur, and (c) over South Asia (60-95°E, 0-30°N), respectively. The column-mean uncertainty in CALIPSO extinction data is  $\pm 110\%$ ,  $\pm 93\%$ , and  $\pm 91\%$  in panels (a)-(c); Percent differences between the simulated and CALIPSO profiles are shown for (d) Nainital, (e) Kanpur, and (f) South Asia.

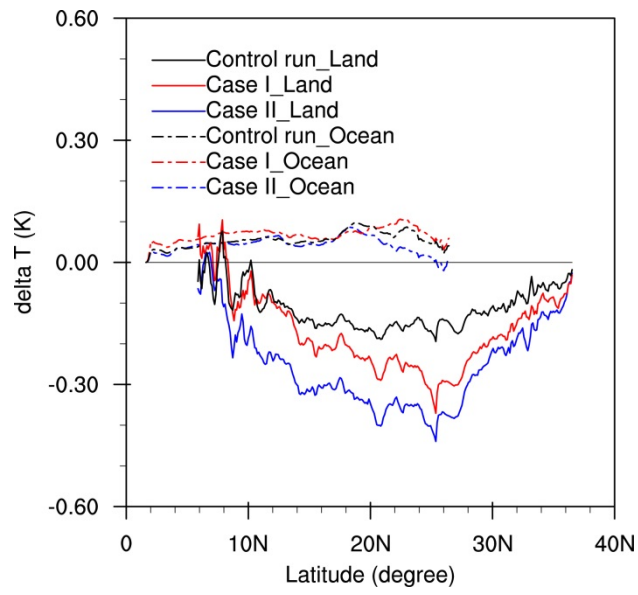


**Figure 3.** Changes in surface air temperature (K) due to aerosol radiative effects for three model simulations.

975

976

977

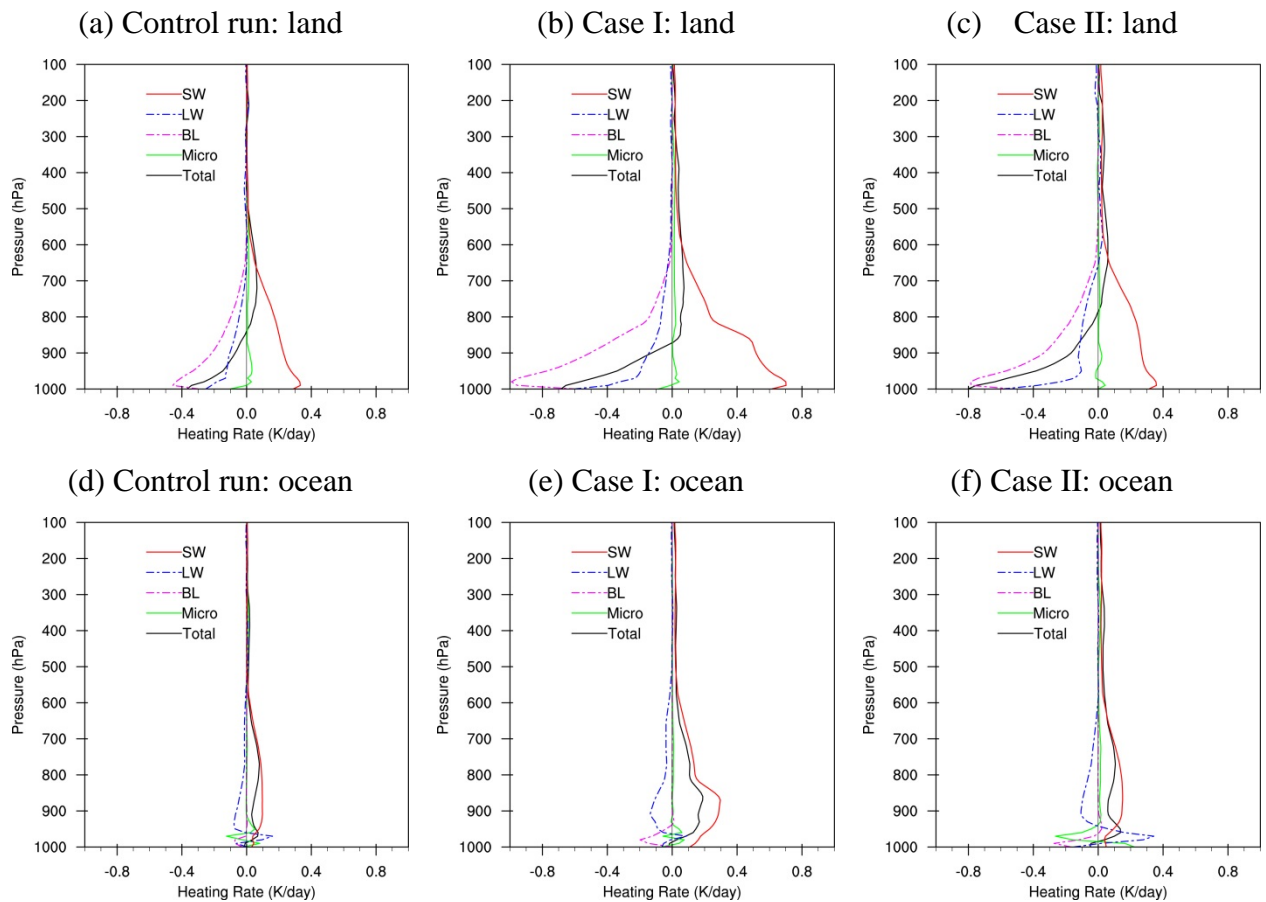


**Figure 4.** Calculated monthly mean heating rates (temperature tendency,  $dT/dt$ , in K/day) perturbed by aerosols, over land for (a) the control run, (b) Case I, and (c) Case II, as well as over the ocean for (d) the control run, (e) Case I, and (f) Case II. The heating processes include shortwave (SW) radiation (red), longwave (LW) radiation (blue dashed), boundary mixing (BL; magenta dashed), and cloud microphysics (Micro; green). The total heating due to aerosol effects is shown with solid black lines.



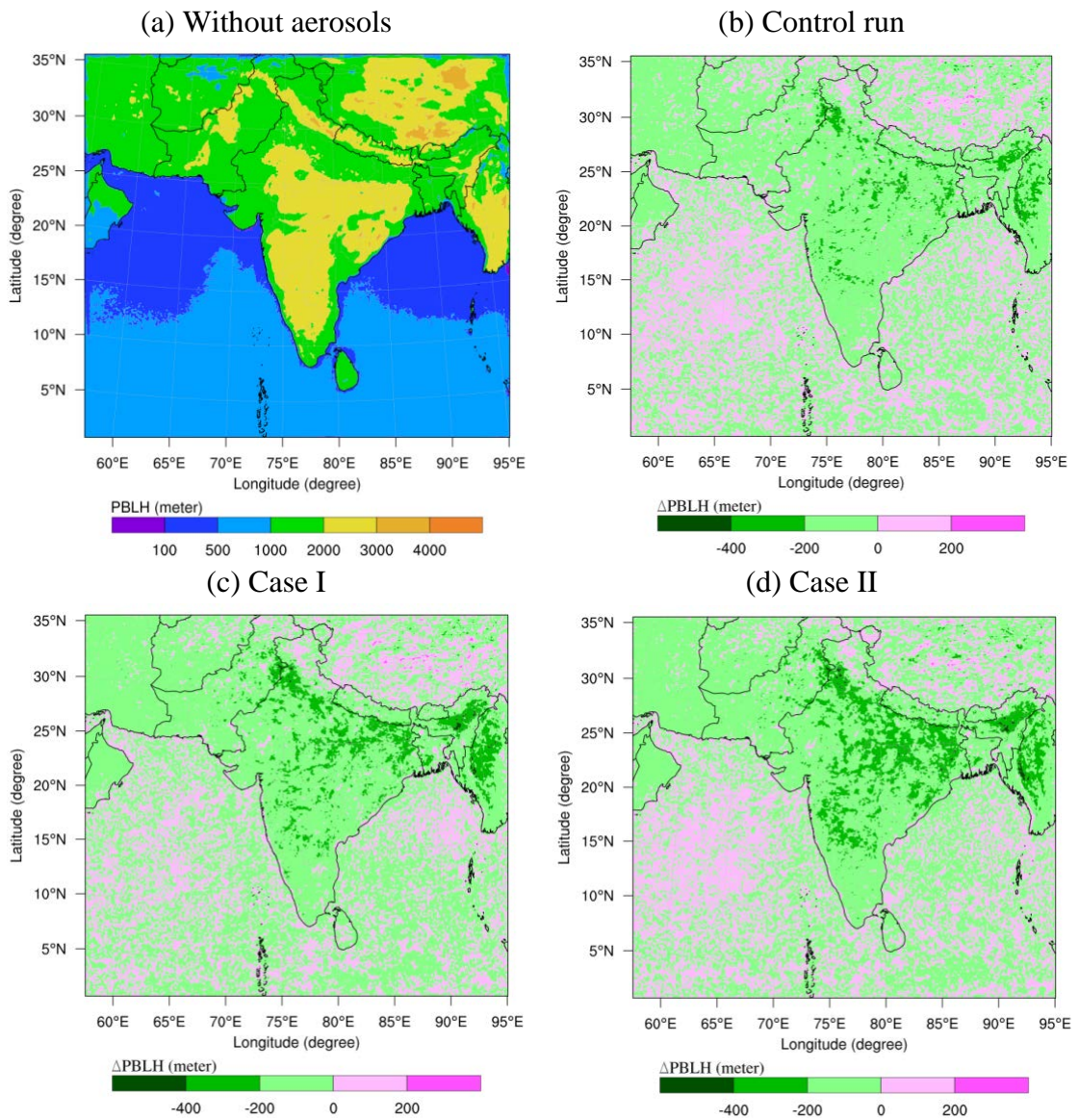


**Figure 5.** (a) Calculated monthly mean planetary BL height (PBLH) at 1300-1400 local time for March, without aerosols; and estimated changes in PBLH ( $\Delta$ PBLH) due to aerosols in (b) the control run, (c) Case I, and (d) Case II.

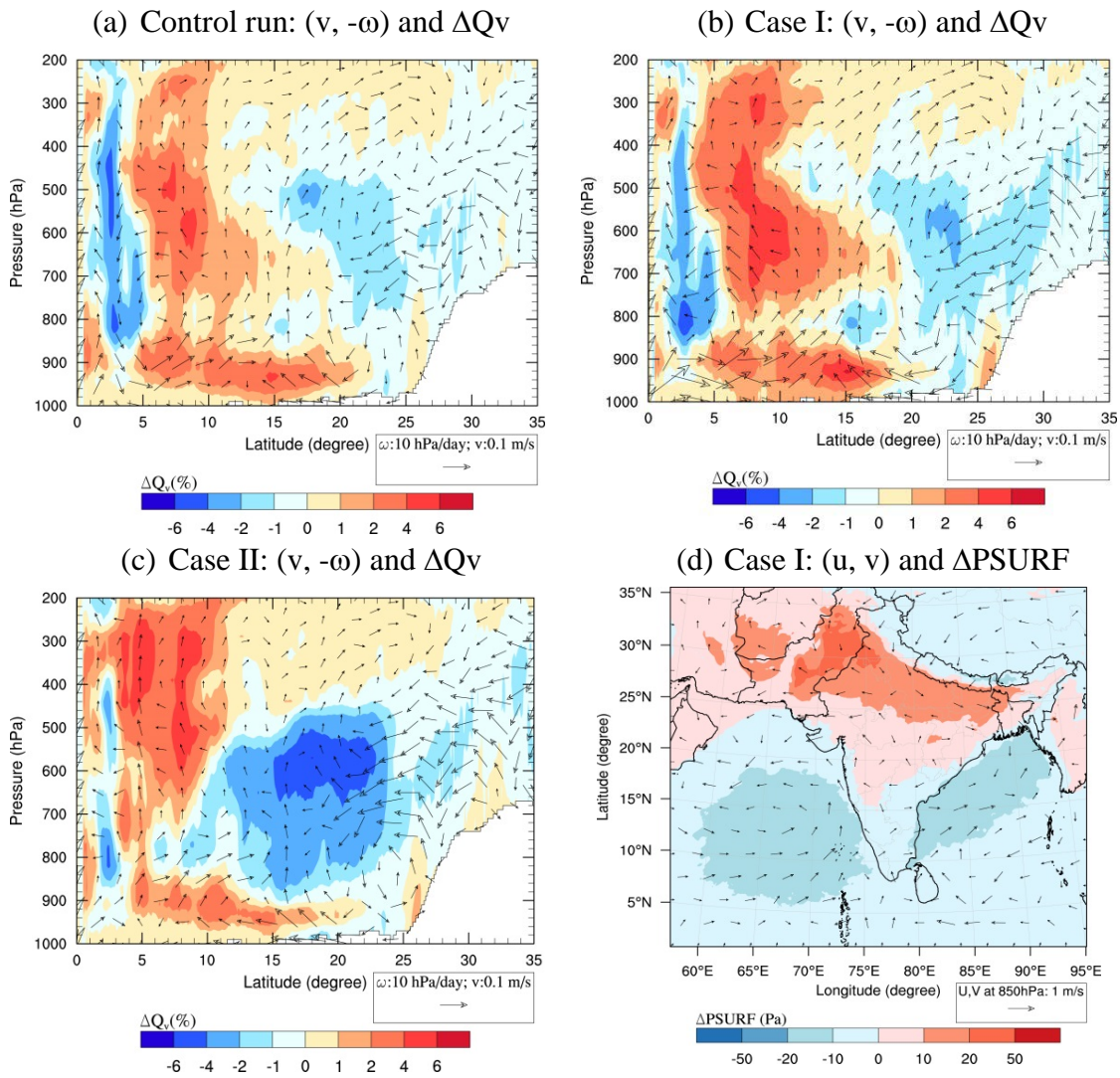


**Figure 6.** Changes in meridional circulation ( $v, -\omega$ ), averaged at  $60-95^\circ\text{E}$ , due to different aerosol effects for (a) the control run, (b) Case I, and (c) Case II, where  $v$  (scaled to  $0.1 \text{ m/s}$ ) is the meridional velocity, and  $-\omega$  (scaled to  $10 \text{ hPa/day}$ ) is the vertical velocity. The color-shaded contours in the background indicate the changes (%) in total precipitable water ( $\Delta Qv$ ) in the column due to aerosols. Panel (d) shows the changes in horizontal winds ( $u, v$ ) at  $850 \text{ hPa}$  and surface pressure changes ( $\Delta PSURF$ ) due to aerosols for Case I.

985

986

987

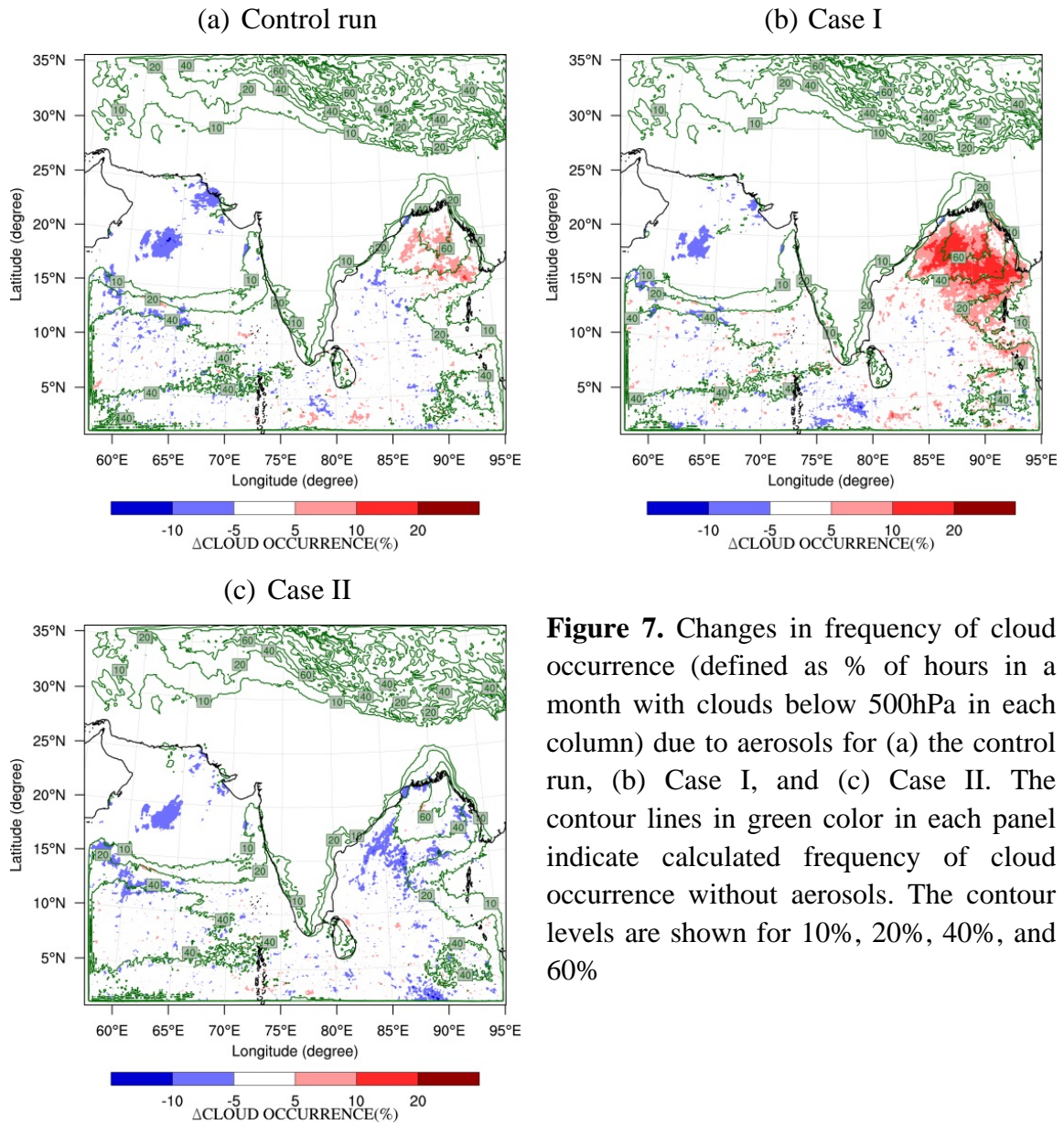


**Figure 7.** Changes in frequency of cloud occurrence (defined as % of hours in a month with clouds below 500hPa in each column) due to aerosols for (a) the control run, (b) Case I, and (c) Case II. The contour lines in green color in each panel indicate calculated frequency of cloud occurrence without aerosols. The contour levels are shown for 10%, 20%, 40%, and 60%

## Supplementary Material

### 1. Contributions by individual aerosol species

In our model, aerosol optical depth (AOD) is calculated with internal mixing assumption. In order to attribute the AOD underestimation to major aerosol types, we plot the species-specific aerosol burdens as a proxy for understanding the contribution to the AOD by individual aerosol species. Fig. S1 shows the aerosol burdens calculated for March 2012. Dust is the dominating species over northwestern India semi-arid regions and the adjacent Arabian Sea, and could be the main contributor to the underestimation of AOD over these regions. In contrast, anthropogenic sulfate, oc, and bc contribute to the main composition of aerosols (thus AOD) in northern and northeastern India, as well as in the long-distance transported aerosols over the downwind of southwestern Indian sub-continent.

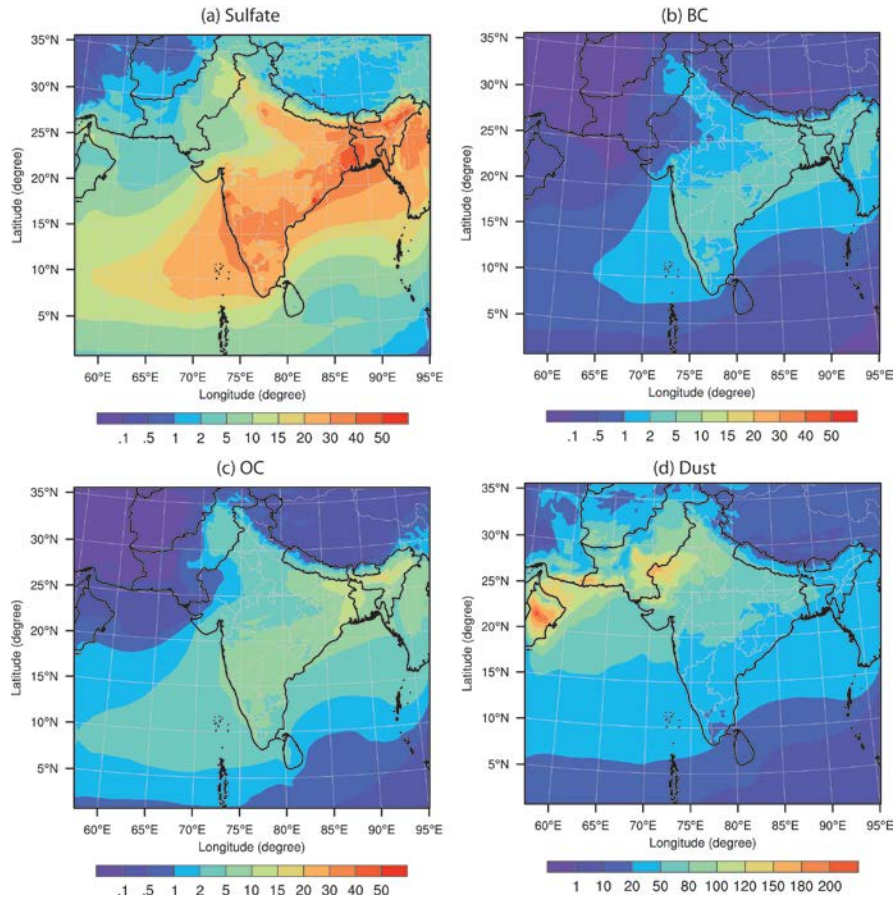


Figure S1. Calculated aerosol burdens ( $\text{mg}/\text{m}^2$ ) of (a) Sulfate, (b) BC, (c) OC, and (d) Dust for March 2012

### 2. Comparison of time averaged AOD between August 2011 and March 2012

The figure shows the time-averaged AOD calculated from the 8-month WRF-Chem simulations in comparison with the MODIS satellite retrievals between August 2011 and March 2012. It indicates underestimation in the model-calculated AOD similar to that for March 2012. We focus on the AOD and

extinction comparisons for March 2012, because the ground-based lidar observations of aerosol vertical profiles are available only for that month. Resolving the mismatch between simulated and observed AOD and extinction profiles requires possible upgrades of multiple model physics schemes and quantification of key parameters that could affect vertical distribution of aerosols, for instance, aerosol emissions, biomass burning injection heights (Grell et al., 2011), boundary layer height and near-surface winds (Nair et al., 2012). Additionally, high-quality measurements at different locations are also needed for model evaluation over longer time periods, and it is recommended for future studies over this region.

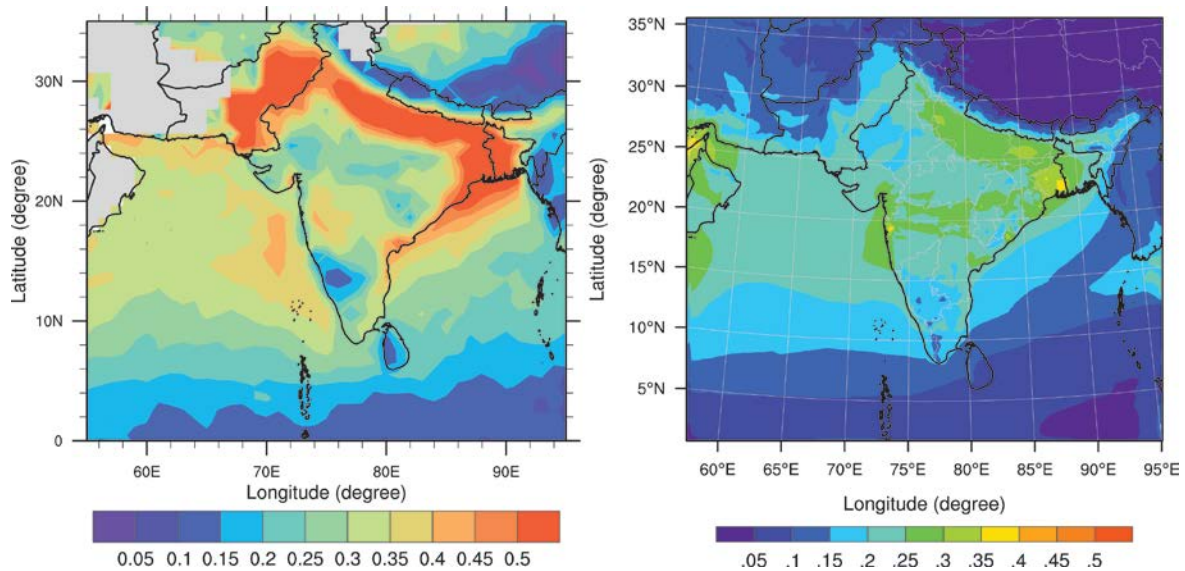


Figure S2. Time averaged AOD between Aug 2011 and March 2012 from (left) MODIS/Terra, and (right) WRF-Chem simulations